DØ Search for Neutral Higgs Bosons at High $\tan\beta$ in multi-jet Events using p17 Data

Fabrice Couderc, Marine Michaut, Boris Tuchming
Dapnia/Spp, Saclay
Per Jonsson, Stephen Robinson, Tim Scanlon
Imperial College, London

Abstract

The full RunIIa data sample recorded at DØ has been analyzed to search for Neutral Higgs bosons produced in association with b-quarks at high $\tan\beta$ within the MSSM framework. The search has been performed in the three b-quarks channel using multi-jet triggered events corresponding to an integrated luminosity of ~ 0.9 fb^{-1}. No excess of events with respect to the predicted background is observed in the final selected three b-tag sample, so that limits are set in the MSSM parameter space.

Contents

Introduction

In this note, we describe the search for the final state $h(\rightarrow b\overline{b})b(b)$ in $p\overline{p}$ collisions at a center of mass energy of 1960 GeV, using 0.9 fb^{-1} of data recorded by the DØ experiment at the Tevatron collider. This associated Higgs boson production is particularly relevant in supersymmetric models where its production cross section could be enhanced compared to the standard model one.

1 Higgs sector in the MSSM

While in the standard model (SM) only one Higgs doublet is required to break the SU(2) symmetry, in Supersymmetric (SUSY) theories, at least two Higgs doublet are necessary (to cancel triangular anomalies). After the electroweak symmetry breaking, 5 Higgs bosons remains. Three of them are neutral bosons : h, H (scalar) and A (pseudo-scalar), and two are charged bosons : H^+ and H^-.

The Higgs sector in the MSSM can be parametrized with respect to $\tan\beta$ (ratio of the two Higgs double vacuum expectation values) and m_A (mass of the pseudo-scalar Higgs A). Figure 1 shows the m_h and m_H value versus the A mass for different $\tan\beta$ values and in different MSSM scenarii. One can see in this figure that m_h has a maximum value m_h^{max}, that $m_H > m_h^{max}$. One can also notice from this figure that the high $\tan\beta$ value area is an interesting case with the following properties :

- $m_A < m_h^{max}$: $m_h \approx m_A$ and $m_H \approx m_h^{max}$
- $m_A > m_h^{max}$: $m_H \approx m_A$ and $m_h \approx m_h^{max}$

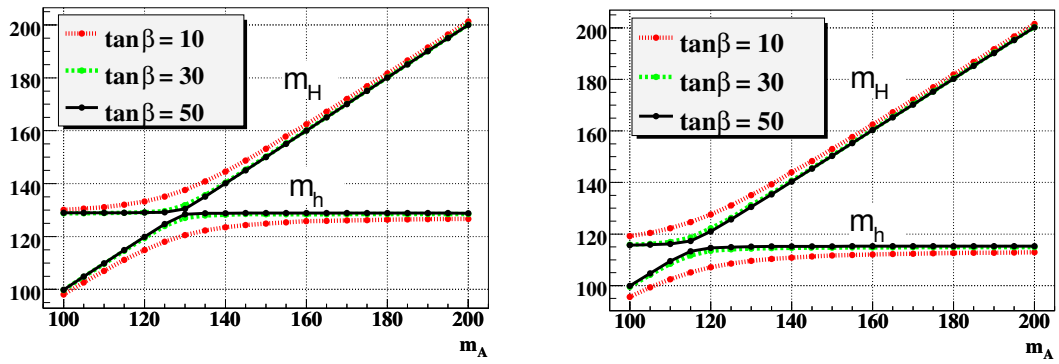

Figure 1: Higgs bosons h, H masses versus m_A for 3 values of $\tan\beta$ and in two benchmark MSSM scenarii : maximal mixing (left), no mixing (right).

Though $\tan\beta$ is a free parameter of the different MSSM, several reasons lead to believe that $\tan\beta$ might be large. A value of $\tan\beta \approx 35$ naturally explains the top bottom quarks mass difference. High $\tan\beta$ values would also provide a good explanation to the density of Dark Matter observed in the universe.

1.1 Higgs coupling to quarks in the MSSM

The Higgs coupling to quarks in the MSSM is proportional to the corresponding one in the SM. The proportionality factor depends on the type of the quark (up or down) and on the type of the Higgs boson. This couplings are summarized in Table 1. In this table, the parameter α comes from the Higgs mass matrix diagonalization, this is a mixing parameter.

Higgs boson	up quarks	down quarks
h	$+\frac{\cos\alpha}{\sin\beta}$	$-\frac{\sin\alpha}{\cos\beta}$
H	$+\frac{\sin\alpha}{\sin\beta}$	$-\frac{\cos\alpha}{\cos\beta}$
A	$+\mathrm{cotan}\,\beta$	$-\tan\beta$

Table 1: MSSM Higgs couplings to quarks.

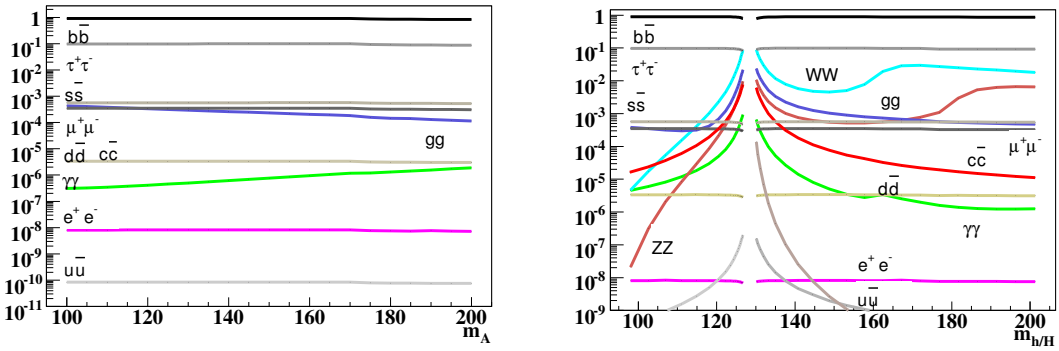

Figure 2: Branching fractions of the A Higgs bosons (left) and h, H Higgs bosons (right) to several final states int the scenario maximal mixing and $\tan\beta = 10$.

One can show that in the high $\tan\beta$ limit case, either the coupling of down quarks to h when $m_A < m_h^{max}$, or the coupling of down quarks to H, when $m_A > m_h^{max}$ is enhanced by $\tan\beta$. Thus two Higgs bosons ($A + h$ or $A + H$) with approximately the same mass have a coupling enhanced by $\tan\beta$ compared to the SM one, while the coupling to up quarks is suppressed. Therefore, in these cases the production of Higgs bosons associated with bottom quarks (highest mass of the down quarks) becomes very interesting: while in the SM, this process cross-section is very low, in the MSSM it is enhanced by an important factor $2 \times \tan^2\beta$.

At high $\tan\beta$, the three Higgs boson couplings actually follow the sum rule $g^2_{hbb} + g^2_{Hbb} + g^2_{Abb} \approx 2 \times \tan\beta^2$. So when the three Higgs boson masses are degenerated, $m_A \approx m_h \approx m_H \approx m_h^{max}$, we also have the same enhancement factor of $2 \times \tan^2\beta$ for the total production of h, H and A associated with bottom quarks.

1.2 MSSM Higgs boson decays

Figure 2 provides insight into the $\Phi \equiv h, H, A$ decay mechanisms. Due to the $\tan\beta$ enhancement, the main decay is, for all these bosons, $\Phi \to b\overline{b}$ ($\mathcal{B}(\Phi \to b\overline{b}) \approx 90$ %).

As a conclusion, we will concentrate in this analysis on Higgs boson production associated with b quarks. The Higgs will be reconstructed in its decay $h \to b\overline{b}$. We will optimize the analysis using a SM simulation of the process $p + \overline{p} \to hb$ and assume that the MSSM cross section is enhanced by a factor $2 \times \tan^2\beta$ compared to the SM model one but still has the same topology and backgrounds.

1.3 hb production in the standard model

The final state $hb(\overline{b})$ is the result of the LO process : $gb \rightarrow hb$ [1] shown in Figure 3, this is called the 5 flavor scheme. Another scheme exists, called the 4 flavor scheme, which is $gg \rightarrow b\overline{b}h$ (also display on Figure 3). Both approaches lead to equivalent results. This is demonstrated in Figure 4. For simplicity, we will only study the 5 flavor scheme.

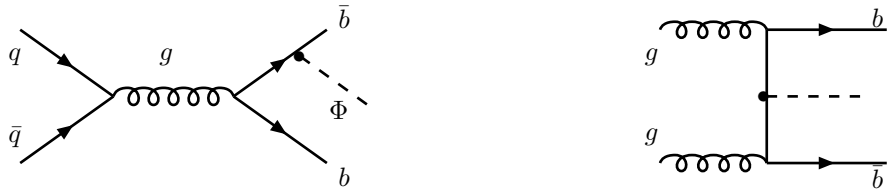

(a) 4 favor scheme

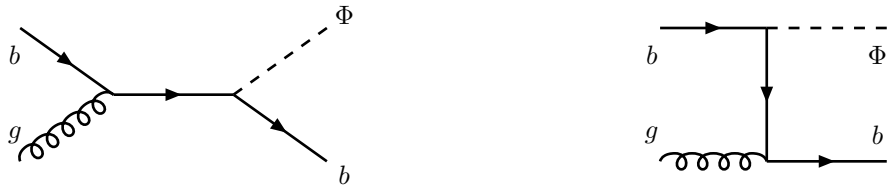

(b) 5 flavor scheme

Figure 3: Feynman diagrams contributing to the LO $hb(b)$ production in $p\overline{p}$ collisions. Φ is either h,H or A.

1.4 "State of the Art"

So far, the MSSM Higgs production has been studied at LEP which excluded at 95 % CL $m_{h,A} < 93$ GeV/c^2 for all $\tan\beta$ values [2]. CDF [3] and then DØ [4, 5] has extended the MSSM Higgs boson mass searches at higher mass. The current DØ limits available at tree level in the $(\tan\beta, m_A)$ are shown in figure 5.

The current best limits available in the $(\tan\beta, m_A)$ plane are summarized on Figure 6 for two SUSY scenarii :

- the so-called m_h^{max} scenario which is defined by the MSSM parameters : $M_{SUSY} = 1$ TeV, $X_t = 2$ TeV, $M_2 = |\mu| = 0.2$ TeV and $m_g = 0.8$ TeV,
- and the no-mixing scenario : $M_{SUSY} = 1$ TeV, $X_t = 0$ TeV, $M_2 = |\mu| = 0.2$ TeV and $m_g = 1.6$ TeV.

[1] in the following h will refer to h, H or A

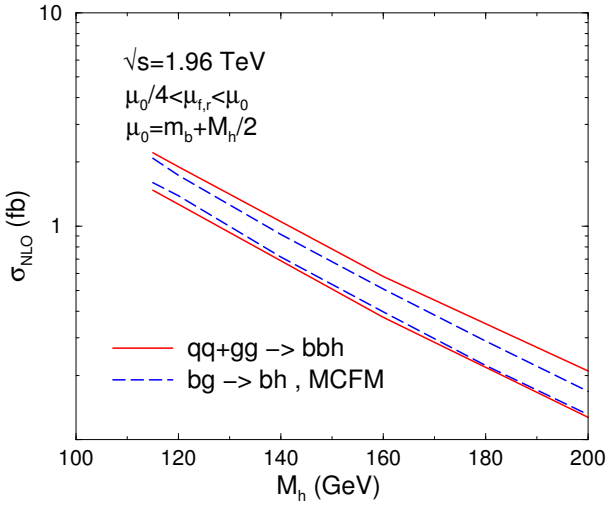

Figure 4: Cross sections of the process $p\overline{p} \to hb(\overline{b})$ in the 5 flavor and 4 flavor schemes [1].

They include LEP results as well as two different kinds of analysis for the Tevatron, results from DØ obtained from a search of the $h(\to bb)b$ final state [4], and results from CDF ([6]) and DØ ([7]) obtained from a search in the $h(\to \tau\tau)$ final state.

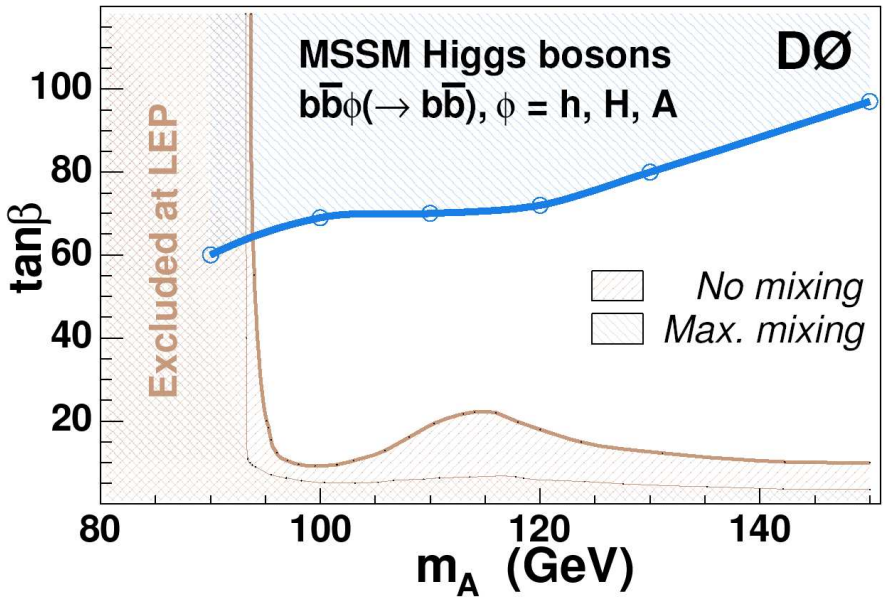

Figure 5: The current DØ observed 95 % CL limits on $\tan\beta$ as a function of m_A at tree level, i.e. assuming a $\tan\beta^2$ cross section enhancement [4, 5]. Around 300 pb^{-1} are analyzed.

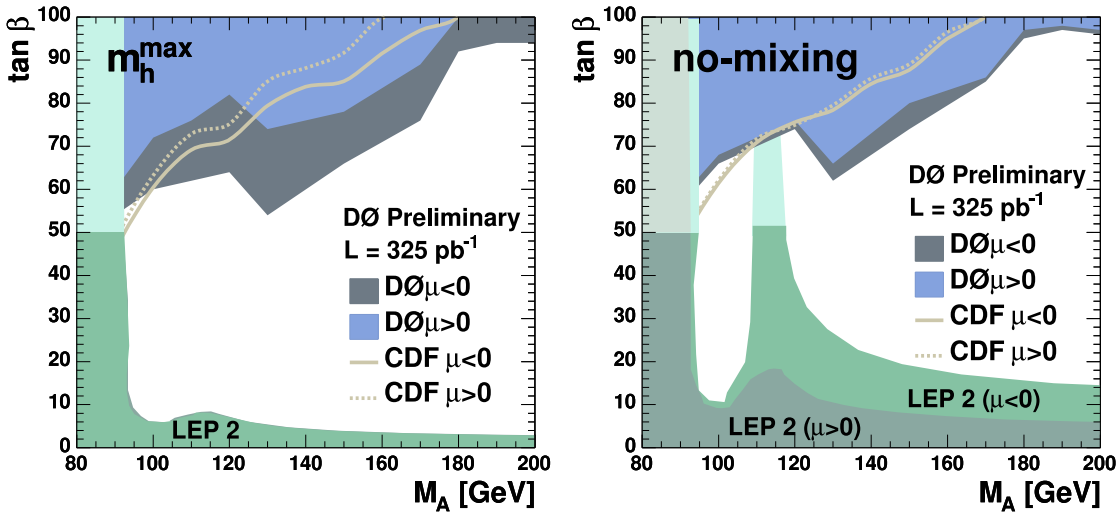

Figure 6: Combined limits in $(\tan\beta, m_A)$ plane in the tow benchmark scenarii: m_h^{max} on the left and no-mixing on the right.

2 Event simulation

Events where generated using the p17.09.01 full simulation chain, including zero bias event overlay, followed by the p17.09.05 refixing and the production of CAFTrees [18]. At the generator level, Pythia [8] or ALPGEN [19] have been run with the PDF set CTEQ6L1.

2.1 Correction to full simulation

To correct for discrepancy between DØ simulation and the real data, we have been using the standard tool implemented as cafe [18] packages:

- We use the b-tagging tag rate function provided by the b-id group, as weight factors, to simulate b-tagging efficiency on b-jets and on light jets
- We use the "Smeared Shift and Removed" (SSR) method to correct for jet-id efficiency, jet energy scale difference between data and MC, and resolution. [20]

In addition, trigger efficiencies (see Section 4) have been measured and are simulated using macros in the higgs_hb package. In the same way, taggability of jets has been measured in the data and is applied as a weight on simulated events (see Section 3.2.3).

2.2 hb Signal simulation

As the main difference between the MSSM Higgs bosons and the SM Higgs boson is the enhancement of the cross-section production by a factor $\tan^2\beta$, the hb signal is simulated with the Monte Carlo program Pythia using its process $gb \to hb$. However, this simulates only the leading order production corrected by initial and final state radiations. As the process $gb \to hb$ has been calculated at the next-to-leading order [9, 10], this simulation needs to be corrected.

We use the MCFM program [11] to compute the required corrections. Not only we use the $gb \to hb$ cross-section computed by MCFM at the next-to-leading order (see 2.2.1) instead of the Pythia one, but we also correct the experimental acceptance of the Higgs boson signal by weighting each simulated signal event according to its kinematic parameters (p_T, η).

2.2.1 MCFM simulation of the $gb \to hb$ process

The MCFM cross sections are obtained using CTEQ6L parton distribution functions (PDFs) at the LO and CTEQ6M PDFs at the NLO. The cuts $p_T > 15$ GeV/c and $\eta < 2.5$ on all outgoing partons are required in order to reproduce the experimental acceptance. These kinematic cuts are also used in our Pythia simulation, they do not yield any systematic effects as the actual experimental cuts are on raw p_T's. Therefore, this correspond to a cut on the Jet Energy Scale (JES) corrected p_T of roughly : $p_T > 20$ GeV/c.

The MCFM computations are done in three steps for each result. These steps corresponds to :

- step 1 : NLO computation of the process $gb \to hb(g)$;
- step 2 : real corrections due to the process $gb \to hb(b)$ where the second b can not observed (real means that there is another soft outgoing parton);
- step 3 : real corrections due to the process $gb \to hbb$ where the second b is actually observed.

The choice of the renormalization scale μ_R and factorization scale μ_F (used in the MCFM simulation) has been investigated elsewhere [12, 13] and we fix $\mu \equiv \mu_R = \mu_F = (2m_b + M_h)/4$ motivated by these studies. The dependence of the cross-sections on the renormalization scale is taken as systematic

uncertainty by varying these scale in the range $\mu/2$ to 2μ. Table 2 summarizes the different results we obtained at the LO(μ), NLO(μ), NLO($\mu/2$) and NLO(2μ) for the different Higgs boson masses tested in this analysis.

M_h	σ LO + cteq6L	σ NLO + cteq6M	σ NLO + cteq5M
90	8.66	$10.93 \pm 0.05 \pm 0.22$	12.91
100	5.75	$7.28 \pm 0.03 \pm 0.18$	8.74
110	3.89	$5.00 \pm 0.02 \pm 0.08$	6.01
120	2.69	$3.52 \pm 0.01 \pm 0.09$	4.24
140	1.34	$1.78 \pm 0.01 \pm 0.07$	2.17
150	0.96	$1.29 \pm 0.01 \pm 0.05$	1.59
170	0.51	$0.71 \pm 0.01 \pm 0.03$	0.88

Table 2: SM cross sections for the Process $f1 + f2 \rightarrow gh$. For the NLO results, the first uncertainty is statistical, the second one is systematic and is due to the renormalization and factorization scales. The last row gives the results obtained with the previous cteq5 parametrization as a comparison to our central value obtained with cteq6.

Table 2 also shows what would be obtained with the previous cteq5 parametrization which yields higher cross sections by about 20 %. This effect is expected as the cteq6 parametrization as a harder gluon spectrum than the cteq5 one [14]. To compute the actual uncertainty due to the PDF, we use the 40 eigenvector sets of PDF provided by the cteq collaboration. The effect of these different parametrization off reproducing the same data is taken as systematic uncertainty. This study has been performed only for the $m_H = 100$ GeV/c^2 point. The results obtained for the 40 different sets are displayed on Fig. 7. The overall systematic uncertainty is the quadratic sum of all the variations due to each eigenvector. In this summation, one has to remember that the 40 sets correspond to a the positive and negative variation of 20 orthogonal sources of uncertainty. This yields to a relative systematic uncertainty of : $+10.2$ %, -13.3 %. For convenience, we will use the symetric uncertainty : ± 11.7 %.

2.2.2 Higgs boson kinematic distributions

To obtain the correct experimental acceptance one needs to correct the (p_T, η) distributions of the Higgs boson for the NLO corrections (Pythia is mainly a LO simulation + ISR/FSR). This is done by weighting our Pythia simulation, thus allowing to obtain the distributions computed with MCFM.

Figure 8 shows an example of the Higgs boson p_T distributions obtained with Pythia, MCFM LO and MCFM NLO along with, on the left, the correcting weight obtained as the ratio of the histograms : MCFM NLO divided by Pythia. This example has been obtained with a Higgs boson mass of 100 GeV/c^2. The weights are computed for the following mass : 100, 110, 120, 150 and 170 GeV/c^2. For the first three masses, the Pythia distribution reproduces fairly well the MCFM NLO one and the weight are close to one while for the tow last one, it is much closer to the MCFM LO one. All the weight distributions are shown on Figure 9. The weight distributions depend on the mass of the Higgs boson, especially at high mass. Therefore, the corrections used in the analysis are different.

Figure 10 shows an example of the Higgs boson η distributions obtained with Pythia, MCFM LO and MCFM NLO along with, on the left, the corresponding correcting weight distribution. This example has been obtained with a Higgs mass of 100 GeV/c^2. On Figure 10 one can see that the LO and NLO Higgs boson η distributions are quite different. The distributions obtained with Pythia are closer to the LO ones and the correction factors are significant. Notice that, for a Higgs boson mass of 120 GeV/c^2, there

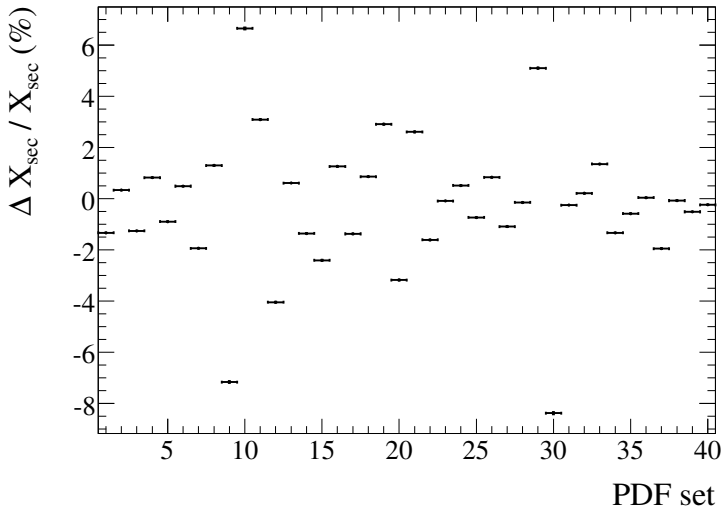

Figure 7: Relative variation of the hb production cross section due to the 40 eigenvector sets of cteq6m pdfs.

is nearly no correction! Figure 11 displays the weight corrections for different Higgs mass.

2.3 Simulation of background events

It should be noticed that the background content of the final selected sample is assessed using real data only. In principle simulating background events is not needed. However it is worthwhile to compare our data to the background simulation. This allows to check if we master the main sources of background events, if the jet resolution, kinematic cuts and trigger thresholds are well understood and modeled in MC.

The main backgrounds for high multiplicity final states with 3 b-tagged jets arise from the QCD multi-jet productions (j stands for light parton):

1. $p\bar{p} \rightarrow jjj(j)$
2. $p\bar{p} \rightarrow bjj(j)$
3. $p\bar{p} \rightarrow b\bar{b}j(j)$
4. $p\bar{p} \rightarrow b\bar{b}b(b)$

The first process is difficult to simulate given the number of diagrams contributing the final state. The processes with b-quark production have been simulated with ALPGEN [19], based on LO matrix elements. A summary of cross-sections obtained with ALPGEN, as well as the kinematic cuts is given in table 2.3.

Numbers are different from the p14 analysis because of following changes:

- PDF set was changed from CTEQ5L to CTEQ6L1. This roughly increases the yields by $\simeq 10\%$.

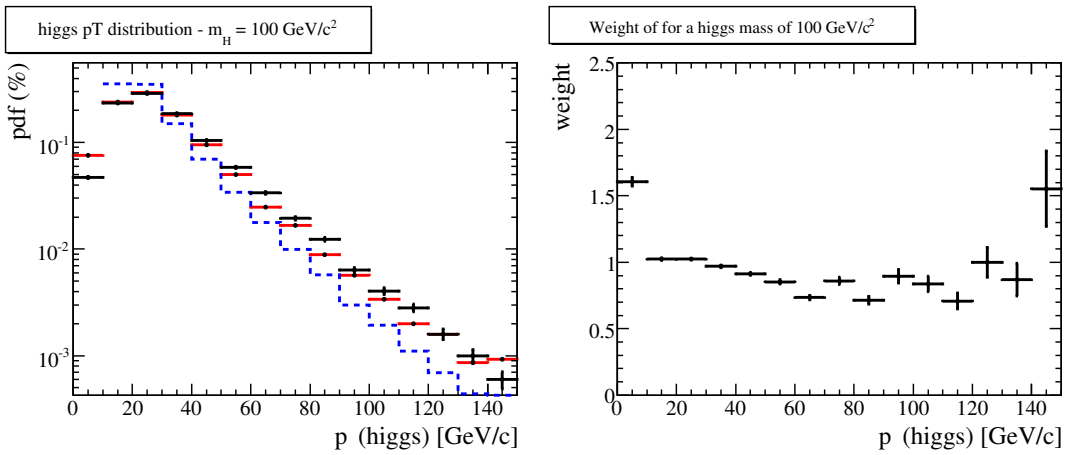

Figure 8: Left : Higgs boson p_T distributions obtained in our Pythia simulation (black), MCFM LO (dashed blue), MCFM NLO (red). Right : correction to the Pythia distribution required to obtain the MCFM NLO distribution.

Process	Cross-section (pb)	Generator cuts (p_T in GeV)
$bbjj$ inclusive	2540	$p_T(j) > 15$, $p_T(b) > 25$, $\|\eta\| < 3$, $\Delta R < 0.4$
$b\bar{b}j$ exclusive	3810	$p_T(j) > 15$, $p_T(b) > 25$ $\|\eta\| < 3$, $\Delta R < 0.4$
$b\bar{b}b\bar{b}$ inclusive	120	2 b's with $p_T(b) > 25$ 3b's with $p_T(b) > 15$

Table 3: cross-section for the generated background events

- Default Q^2 of ALPGEN (renormalization and factorization) has been switched from $Q^2 = \frac{1}{N_{part}} \sum p_T^2$ to $Q^2 = \sum p_T^2$. The impact of this change is a decrease by $\simeq 50\%$ of the cross-sections for the three processes. None of these two possible choices of scale is better than the other one and these variations demonstrate that the uncertainty due to higher order corrections is at the level of $^{+100\%}_{-50\%}$ for the cross-sections quoted in Table 2.3.

- implementation of MLM matching [21] to avoid double counting of events between samples.

- The kinematic cuts for the 4b process have been changed from the common $p_T(b) > 15$ GeV to asymmetric cuts. We demand 2 b-quarks with $p_T > 25$ and 3 b-quarks with $p_T > 15$. The aim was to account for possible irreducible "three b-jets background" that may occur when one of the four b-quarks is very soft and does not produce a reconstructed jets.

  To generate these events a private version of ALPGEN linked to the package d0_mess was build (stored into CVS as of version v01-06-00 of package alpgen_prod). The asymmetric parton-level cuts are performed by d0_mess after relaxing ALPGEN generator cuts.

Simulation of other sources of backgrounds such as $Z + b$ or $t\bar{t}$ productions are not necessary, as their cross-sections are much smaller than the uncertainty arising from the choice of the scale in QCD processes.

2.4 Simulated sample summary

Table 4 gives the number of events simulated for each signal and background processes.

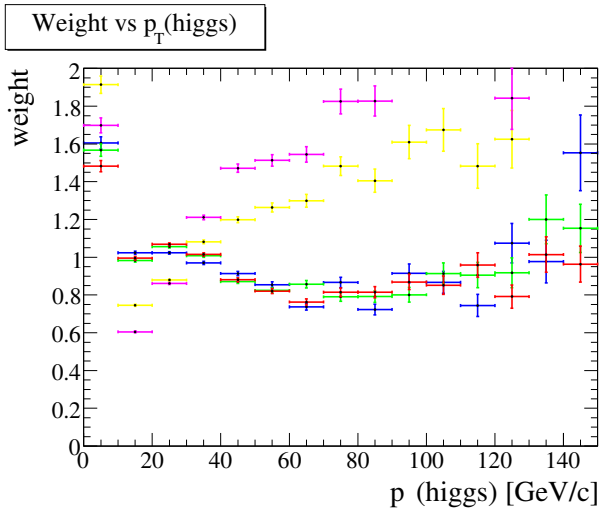

Figure 9: p_T weight distributions obtained in different Higgs boson mass cases : $M_h = 100$ GeV/c^2 (blue), $M_h = 110$ GeV/c^2 (green), $M_h = 120$ GeV/c^2 (red), $M_h = 150$ GeV/c^2 (yellow) and $M_h = 170$ GeV/c^2 (pink).

M_h	Number of events
100	42287
110	43489
120	41798
150	49253
170	50449

Backgrounds	Number of events
bbj	85963
bbjj	297676
bbb(b)	82700

Table 4: The number of events simulated for each signal and background process.

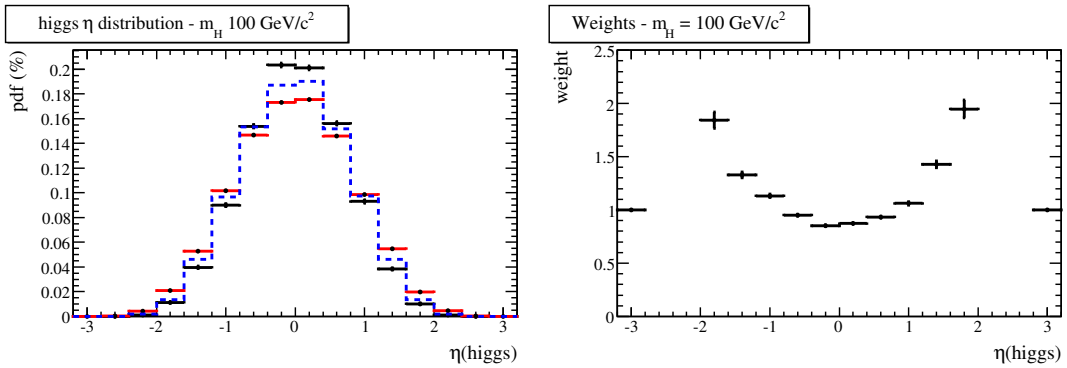

Figure 10: Left : Higgs boson η distributions obtained in our Pythia simulation (black), MCFM LO (dashed blue), MCFM NLO (red). Right : correction to the Pythia distribution required to obtain the MCFM NLO distribution.

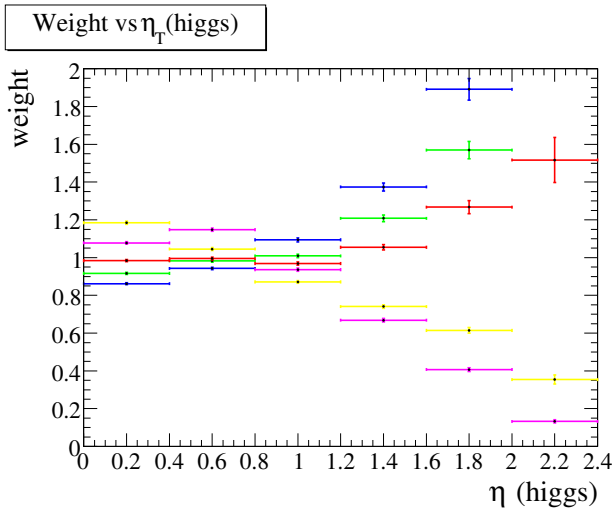

Figure 11: η weight distributions obtained in different Higgs boson mass cases : $M_h = 100$ GeV/c^2 (blue), $M_h = 110$ GeV/c^2 (green), $M_h = 120$ GeV/c^2 (red), $M_h = 150$ GeV/c^2 (yellow) and $M_h = 170$ GeV/c^2 (pink).

Trigger List Version	**Integrated luminosity** (pb^{-1})
v9	20.5
v10	8.3
v11	55.4
v12	171.9
v13	328.3
v14	295.7

Table 5: The integrated luminosity reconstructed using each $h^0b\bar{b}$ trigger after exclusion of bad luminosity blocks.

3 Data Sample

The sample consists of data taken from November 2002 to April 2006 reconstructed with p17 versions of d0reco. about 75% of the data were processed with p17.03 then fixed with p17.05 then refixed with p17.09.03 and 25% of the data were processed with p17.09.01.

Events were first selected using 3JET skim definition. It demands one JCCB jet reconstructed with $\mathrm{P_T} > 20$ GeV and two others with $\mathrm{P_T} > 15$ GeV. These jets have to be within $|\eta| < 2.6$.. The skimming cuts are applied to the data before the jet energy scale corrections. So the same cuts have been simulated for the Monte Carlo events using the package jetcor in mode standalone.

From the 3JET skim, CAFTrees were produced within p18.05.00 version of DØ software. CAFTrees were then processed through the higgs_hb package within p18.07.00. JES and b-tagging were reapplied in order to use certified versions. Certified bad luminosity block list (from dq_def and lm_acess run for $h^0b\bar{b}$ trigger) and detector (Muon, Calorimeter, SMT, CFT) good run list (from caf_dq) are used. This selection rejects 32 % of events. About 75 millions events remain in the sample.

Only events which fired the $h^0b\bar{b}$ triggers described in Table 7 were included in the analysis. The integrated luminosities for all trigger versions, after exclusion of bad luminosity blocks, are shown in Table 5.

3.1 Data Quality Checks

Flags rejecting events which are subject to known calorimeter issues significantly affecting the data quality were applied event by event. Figure 12 shows the properties of the jets in the data sample. There are neither significant spikes nor bumps in the $\mathrm{P_T}$ and η spectra which would be signs of remaining detector problems.

The $\eta - \phi$ distributions of the jets after requiring various numbers of b-tagged jets in the event is also shown in Figure 13. No irregularities are observed.

3.2 Object identifications

3.2.1 Jet Selection

Jets are reconstructed with the RunII Improved Legacy Cone Algorithm and required to pass selection cuts, which allow to eliminate fake jets and EM object.

The jet ID cuts for p17 data have been optimized compared to p14. The details of the optimization can be found in [24]. A brief description of the cuts is given in the following.
The jet has to fulfill a cut on its coarse hadronic fraction (CHF):

- it has CHF < 0.4 or
- it has CHF < 0.6 and $8.5 < \eta^{\mathrm{det}} < 12.5$ and $\mathrm{n_{90}} < 20$, or

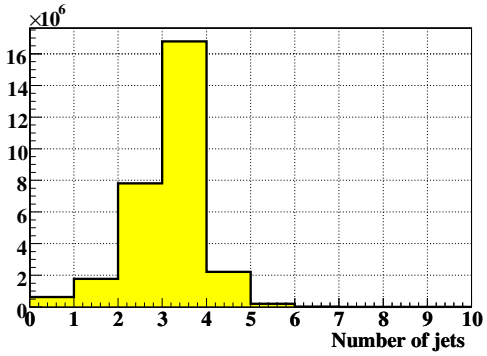

(a) Number of jets

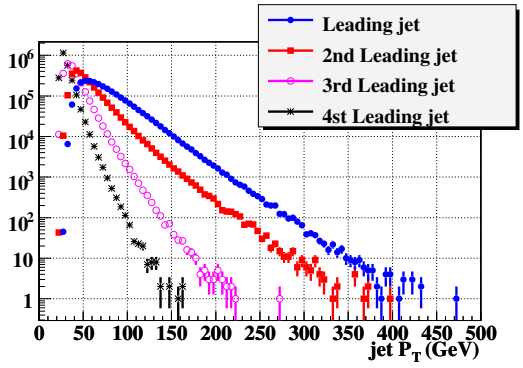

(b) Transverse impulsion of the 4 leading jets

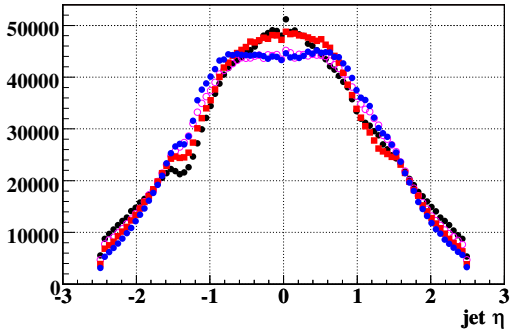

(c) Pseudo rapidity of the 4 leading jets

Figure 12: Basic jet distribution. For each plot, jets must pass quality cuts and taggability requirements, each event must pass $h^0 b\bar{b}$ trigger, the transverse momentum are corrected for jet energy scale, and the three leading jets must have a transverse momentum above 40, 25 and 15 GeV.

- it has CHF < 0.44 and $\eta < 0.8$, or
- it has CHF < 0.46 and $1.5 < \eta < 2.5$.

The jet has also to pass a cut on its electromagnetic fraction (EMF):

- it has EMF > 0.05 or
- it has $1.3 > ||\eta^{\mathrm{det}}| - 12.5| + \max(0, 40 \times (\sigma_\eta - 0.1))$ or
- it has EMF > 0.03 and $11 < |\eta^{\mathrm{det}}| < 14$, or
- it has EMF > 0.04 and $2.5 < |\eta|$.

Finally, the jet has to be confirmed at trigger level:

- it has $\mathrm{L1}_{\mathrm{SET}} > 0.5$, or

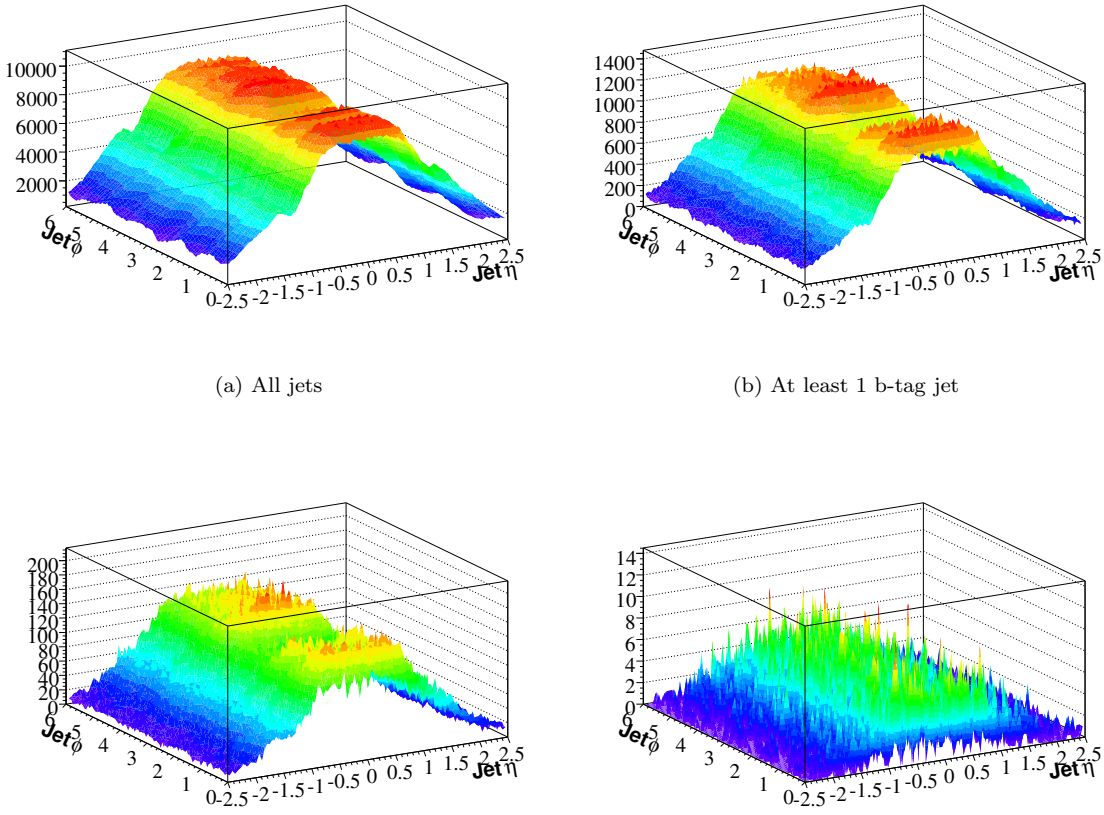

(a) All jets

(b) At least 1 b-tag jet

(c) At least 2 b-tag jets

(d) At least 3 b-tag jets

Figure 13: The $\eta - \phi$ distributions of each jet in event with 0 b-tag, at least 1, 2 or 3 b-tag.

- it has $\mathrm{L1_{SET}} > 0.35$ and $\mathrm{P_T} < 15$ and $1.4 < |\eta|$, or
- it has $\mathrm{L1_{SET}} > 0.1$ and $\mathrm{P_T} < 15$ and $3 < |\eta|$, or
- it has $\mathrm{L1_{SET}} > 0.2$ and $\mathrm{P_T} \geq 15$ and $3 < |\eta|$.

Furthermore, Jets are required in this analysis to have $|\eta| < 2.5$ and $\mathrm{P_T} > 15$ Gev in order to be able to apply the jet energy scale correction and the b-tagging on them.

3.2.2 Jet Energy Scale

The certified Jet Energy Scale corrections from p18-br-05 were applied to all jets. The correction applied in data and MC are shown in Figure 14.

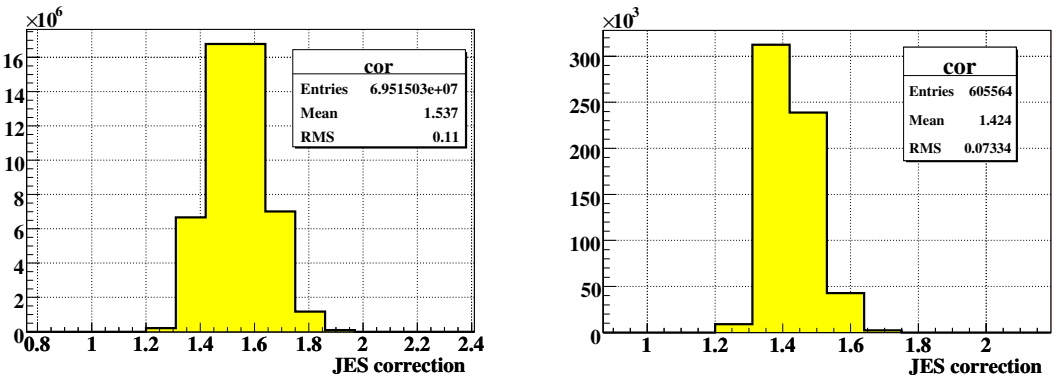

(a) Data (b) Monte Carlo

Figure 14: The jet energy scale correction in data (a) and Monte Carlo (b).

3.2.3 Taggability

Before trying to b-tag jet, a taggability requirement has to be applied. The taggability criteria demands that the calorimeter jet be matched to a track jet ($\Delta R < 0.5$). The track jets are built with good tracks: they must have $p_T > 0.5$ GeV (one of them $p_T > 1$ GeV), hits in the SMT detector and their impact parameters along the beam axis and in the (xy) plane are demanded to be smaller than 0.2 cm and 0.4 cm, respectively.

Since approximately 85% of jets are taggable in data and around 90% in Monte Carlo, we have to take into account the difference. The taggability is measured in the data and parameterized using jet $P_T$and η . The parametrisations are shown in figure 15.

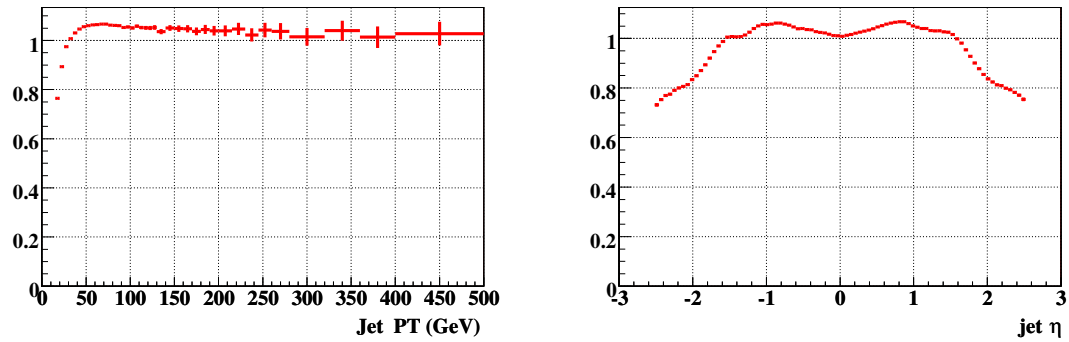

(a) (b)

Figure 15: The taggability parameterization as a function of jet P_T (a), jet η (b).A global scaling factor of 85% has to be applied in addition, since for each of this 1-dimensionnal paramerization, the convolution with the proper distribution is 1.

We use the taggability factor obtained from the data, to randomly decide if a given jet is taggable in the simulation, according to its P_T and its η.

3.2.4 b-Tagging

A pure and efficient identification of jets arising from b quarks is very important in this analysis which selects a final state with at least three b quarks. Significant improvements have been obtained by building a Neural Network b-tagger [25] [26]. The Neural Net tagger took seven input variables from the JLIP, SVT and CSIP b-taggers, such as the decay length significance of the secondary vertex, the weighted combination of the track IP significances, the probability that the jet originates from the primary vertex (PV), the χ^2 per degree of freedom of the secondary vertex, the number of tracks used to reconstruct the secondary vertex, the mass of the secondary vertex and the number of secondary vertices found in the jet. The performance of the NN b-tagger, computed using SystemD method [23] (see section 4), are shown in Figure 16.

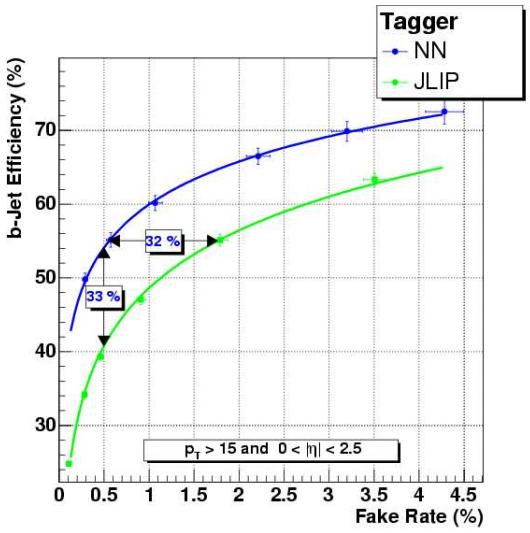

Figure 16: The b-Jet efficiency versus the mist-tag rate for the NN b-tagger (blue) and JLIP b-tagger (green).

One can see that we gain around 30 % in b-jet efficiency with the NN b-tagger compared to JLIP. In this analysis, the "TIGHT" working point is used, and corresponds to a cut on the NN probability above 0.775. The efficiency is in average 48.6 % and the fake rate is in average 0.325 %.
Understanding the possible differences in b-tagging characteristics between data and Monte Carlo is also necessary. tag rate functions, computed from data, one for b-jets and another for light jets, are provided by b-id group to accurately model the data performance in the Monte Carlo. These functions are parameterized in terms of the jet transverse momentum and pseudo-rapidity, and can be seen in Figure 17.

3.3 Selection of candidate events

To further select signal events, a set of analysis cuts are applied:

- the events is required to fire the $h^0 b\bar{b}$ trigger;
- To ensure consistency with the trigger requirements, the z position of the primary vertex is also constrained by $|z_{PV}| < 35$ cm.

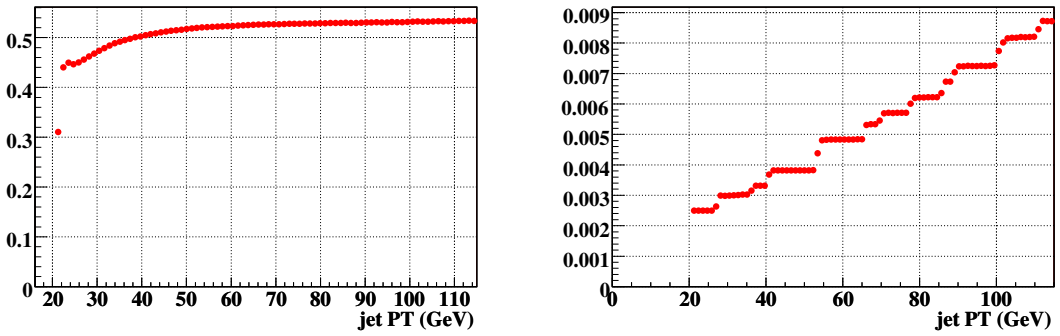

(a) (b)

Figure 17: (a) b-tag efficiency (b) mist-tag rate in 3JET skim versus P_T for the NN tight working point.

	Trigger	Z_{PV} **cut**	**Kinematical**	**BID**
Efficiency	39	95	70	0.04

Table 6: The relative pourcentage of events in data passing each cuts.

- at least three and at max five good and taggable jets with |eta| < 2.5 and $P_T > 15$ GeV (P_T is the raw P_T) are required;
- the jes corrected P_T of the leading jets should be above 40 GeV, of the second leading jet above 25 GeV and of the third leading jet above 15 GeV;
- each event must have at least three Neural Net tight b-tagged jets;

  The table 6 summaries the relative pourcentage of events passing each selection cut.

4 Trigger efficiency

Due to limited bandwidth at trigger level, a set of trigger conditions is used to maximize signal acceptance while keeping trigger rate within available band with up to high luminosity. The data set used in this analysis is taken with six different trigger lists: v9, v10, v11, v12, v13 and v14. The triggering conditions of our trigger for each trigger lists are described in table 1.

Calculating accurately the efficiency of each trigger for signal and backgrounds generated with Monte Carlo is essential. Since no accurate simulation of the DØ calorimeter trigger system is available at the time of this study, significant efforts were devoted to use data to understand trigger performance.

The data set used for this study is based on a muon trigger (each event is required to pass at least one of the muon triggers) in order to have a unbiased sample towards jet triggers. About 10 million events in the CAFTrees TOPJETTRIG were processed with the custom package higgs_hb. Only events with exactly two good jets back to back are kept, with $\Delta\phi(\text{jet}_1 - \text{jet}_2) \geq 2.5$ with $P_T^{cor} > 15$ GeV and $Z_{PV} < 35$ cm.

	v9	**v10**
L1	CJT(4,5,$\|\eta\|<3.2$)	CJT(3,5,$\|\eta\|<3.2$)
L2	JT(3,8,$\|\eta\|<3$)HT(50,5)	same than v9
L3	JT(3,15,$\|\eta\|<3$)	same than v9
Name	3JT15_PV	same than v9

(a) v9 and v10

	v11	**v12**
L1	CJT(3,5,$\|\eta\|<3.2$)	same than v11
L2	JT(3,8,$\|\eta\|<3$)HT(50,5)	same than v11
L3	JT(3,15,$\|\eta\|<3$)JT(2,25,$\|\eta\|<3$) $\|z_{PV}\|<35$ cm	JT(3,15,$\|\eta\|<3$) JT(2,25,$\|\eta\|<3$) $\|z_{PV}\|<35$ cm
Name	3JT15_PV	2J25_3J15_PVZ

(b) v11 and v12

	v13	**v14.0-7**	**v14.8-**
L1	same than v11 et v12	CJT(3,4,$\|\eta\|<2.6$)CJT(3,5,$\|\eta\|<3.2$)	v14.0-7 $*$ CJT(1,7,$\|\eta\|<1.8$)
L2	JT(3,6,$\|\eta\|<3$)HT(70,8)	same than v13	same than v13
L3	v12 $*$ $\text{Prob}_b(0.05)$	same than v13	same than v13
Name	JT2_3JT15_IP_VX	same than v13	same than v13

(c) v13 and v14

Table 7: The triggering conditions for each version of the $h^0 b\bar{b}$ trigger. The CJT(x,y,$|\eta|<$ z) term corresponds to x calorimeter trigger towers above y GeV and within $|\eta|<$ z. The JT(x,y,$|\eta|<$ z) term corresponds to x jets reconstructed at L2 or L3 with $P_T >$ y GeV and $|\eta|<$ z. The HT(x,y) term is used only at L2 and requires that the transverse momentum of L2 jets with $P_T >$ y GeV is above x GeV. The $\text{Prob}_b(0.05)$ term is used only at L3 and corresponds to have a probability for the event to have no jet less than 0.05.

The probability P(L1,L2,L3) is computed for each signal or background event using:

$$\mathrm{P(L1,L2,L3)} = \mathrm{P(L1)} \times \mathrm{P(L2 \mid L1)} \times \mathrm{P(L3 \mid L1,L2)}$$

where P(N2 | N1) and P(N3 | N1, N2) are the conditional probabilities to fire the trigger conditions of a particular level when the previous levels are fired.

To take into account the different trigger lists used in the analysis, a weight corresponding to the integrated luminosity taken by each trigger version is applied to each event:

$$\mathrm{P(L1,L2,L3)_{finale}} = \sum_{\mathrm{i=v9,v14}} \mathrm{P(L1,L2,L3)_i} \times \frac{\mathcal{L}_\mathrm{i}}{\mathcal{L}_\mathrm{tot}}$$

The method exposed in the following is inspired by [22] and adapted to v13-14 trigger list.

4.1 Level 1

The number of L1 calorimeter trigger towers above the required thresholds for a particular multi-jet event depends on the properties of each jet in the event. For example, a di-jet event can fire two towers in two different ways: either each jet fires one tower, or one jet fires two towers and the other one fires no tower. Things get even more complicated in v14 trigger list, for which the L1 term requires towers in particular regions of the calorimeter. The method used to compute the efficiency of CJT(x,y,z) can be divided into three steps:

4.1.1 Effect of a jet reconstructed offline on calorimetric trigger towers

The first step consists to measure the effect of a single jet on calorimeter trigger towers. Since we want to include all jet energy within an R = 0.5 cone and since the upper η coverage of the L1 trigger towers is currently 3.2, only jets with $\eta_{\mathrm{jet}}^{\mathrm{det}} < 2.7$ are considered.
To study the effect of single jets, we look at the trigger towers near the jet. Looking at Figure 18 which shows the angular separation between the leading jet and the leading tower, we see that a cut in ΔR of 0.5 should be wide enough to capture leading towers but tight enough to minimize the chance of towers affected by a possible non-reconstructed jet in the event. A tower fired by the jet is then a tower with a transverse energy above threshold within $\Delta\mathrm{R} = 0.5$.

The number of fired towers per jet is measured in the di-jet sample described previously, and stored in a two dimensional histograms with the x axis being the jet corrected $\mathrm{P_T}$ and the y axis the number of towers fired by the jet. To take into account the increasing instantaneous luminosity, each measurement is done in each trigger list, namely v12, v13 and v14 (statistic is too low in v9-11).
To deal with each regional η term of each different trigger list, we need to measure the number of towers per jet satisfying:

1) $\mathrm{P_T^{tower}} \geq 7$ GeV with $\eta^{\mathrm{tower}} < 1.8$; Figure 19 shows the number of towers above 7 GeV within $\eta < 1.8$ versus the $\mathrm{P_T}$ of the jet they are matched to.

2) 5 GeV $< \mathrm{P_T^{tower}} < 7$ GeV with $\eta^{\mathrm{tower}} < 1.8$ or $\mathrm{P_T^{tower}} \geq 5$ GeV with $1.8 \leq \eta^{\mathrm{tower}}$l2.6 while the jet has 0, 1, 2, 3 or more than 4 towers with $\mathrm{P_T^{tower}} \geq 7$ GeV and $\eta^{\mathrm{tower}} < 1.8$; Figure 20 shows the profile plots of the 2D histograms corresponding to the previous trigger terms.

3) 4 GeV $< \mathrm{P_T^{tower}} < 5$ GeV with $|\eta^{\mathrm{tower}}| < 2.6$ while the jet has 0, 1, 2, 3 or more than 4 towers with $\mathrm{P_T^{tower}} \geq 5$ GeV and $\eta^{\mathrm{tower}} < 2.6$; Figure 20 shows the profile plots of the 2D histograms corresponding to the previous trigger terms.

4) $\mathrm{P_T^{tower}} \geq 5$ GeV with $2.6 \leq \eta^{\mathrm{tower}} < 3.2$. Figure 22 shows the 2D histograms corresponding to the previous trigger term.

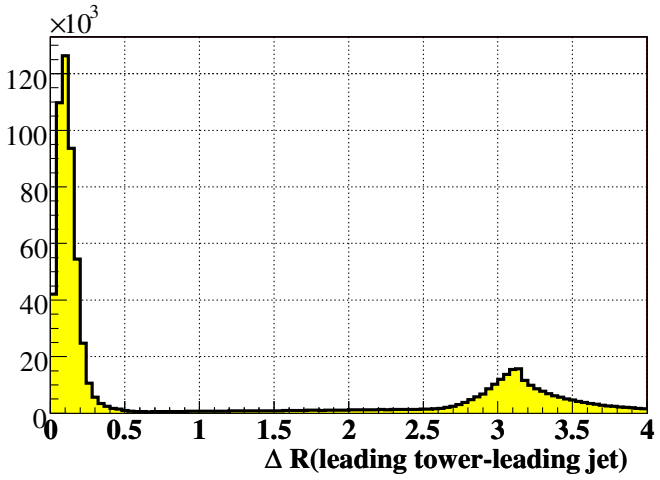

Figure 18: ΔR between the leading tower and the leading jet. A cut at 0.5 is applied.

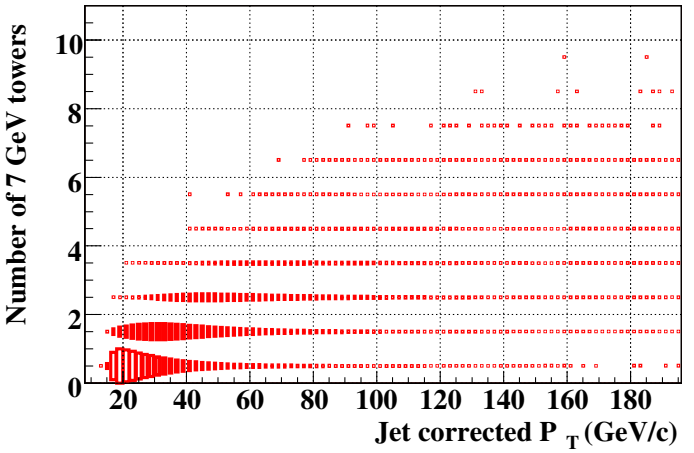

Figure 19: Number of towers above 7 GeV with $\eta < 1.8$ versus corrected jet P_T.

4.1.2 Effect of noise calorimetric trigger towers

The second step is the following: we need to take into account fired towers that are not matched to any reconstructed jet. We will call those towers "noise towers" in the following. They can arise from non-reconstructed jets, electronic noise, pile-up, etc. Since the occurrence of noise towers may depend on instantaneous luminosity, their numbers are measured for each trigger list. To deal with each regional η term, we need to measure the number of noise towers satisfying:

1) $P_T^{tower} \geq 7$ GeV with $\eta^{tower} < 1.8$;

2) 5 GeV $< P_T^{tower} < 7$ GeV with $\eta^{tower} < 1.8$ or $P_T^{tower} \geq 5$ GeV with $1.8 \leq \eta^{tower} < 2.6$;

3) 4 GeV $< P_T^{tower} < 5$ GeV with $\eta^{tower} < 2.6$ or $P_T^{tower} \geq 5$ GeV with $1.8 \leq \eta^{tower} < 2.6$;

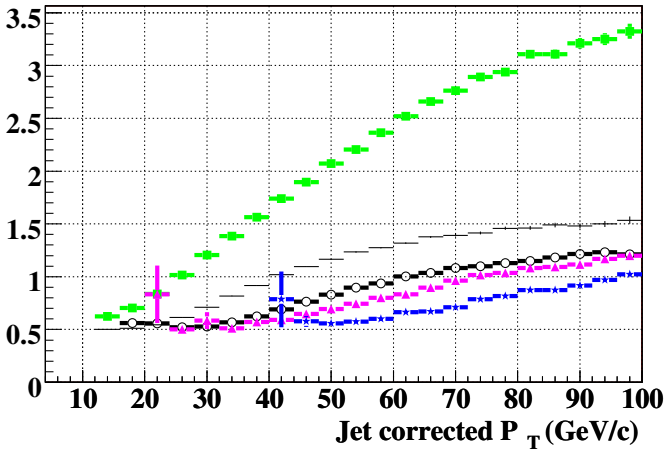

Figure 20: Number of towers between 5 and 7 GeV with $|\eta^{\text{tow}}| < 1.8$ or above 5 GeV with $1.8 \leq |\eta^{\text{tow}}| < 2.6$ versus corrected jet P_T when the jet has 0 (green, square marker), 1 (fine black, no marker), 2 (black, circle marker), 3 (pink, triangle marker) or 4 (blue, star marker) towers above 7 GeV with $|\eta^{\text{tow}}| < 1.8$.

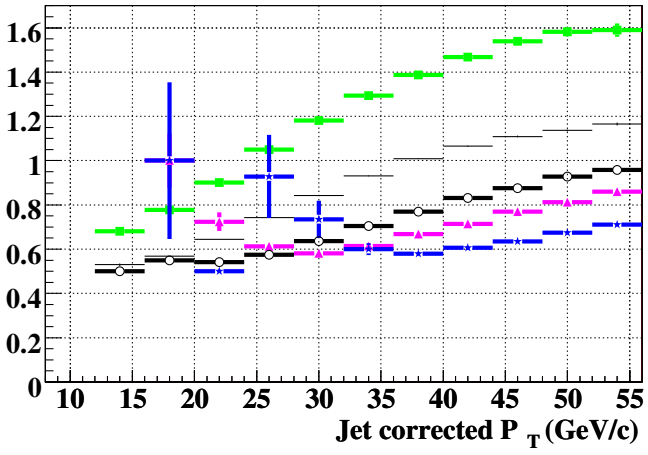

Figure 21: Number of towers above 5 GeV with $|\eta^{\text{tow}}| < 2.6$ versus corrected jet P_T when the jet has 0 (green, square marker), 1 (fine black, no marker), 2 (black, circle marker), 3 (pink, triangle marker) or 4 (blue, star marker) towers above 5 GeV with $|\eta^{\text{tow}}| < 2.6$.

4) $P_T^{\text{tower}} \geq 5$ GeV with $2.6 \leq \eta^{\text{tower}} < 3.2$.

Figure 23 shows the number of noise towers in each calorimeter region in v13 trigger list.

4.1.3 Effect of all jets and noise

The last step consists in combining the effect of all the jets and noise in the event. It can be divided into 3 steps:

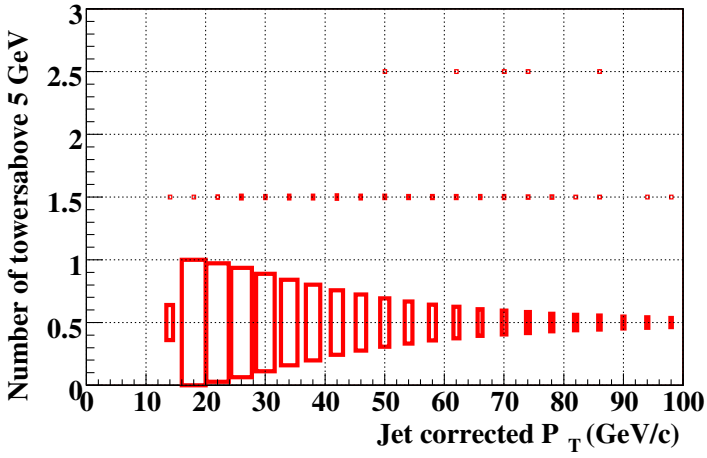

Figure 22: Number of towers above 5 GeV with $2.6 < |\eta^{\text{tow}}| < 3.2$ versus corrected jet P_T.

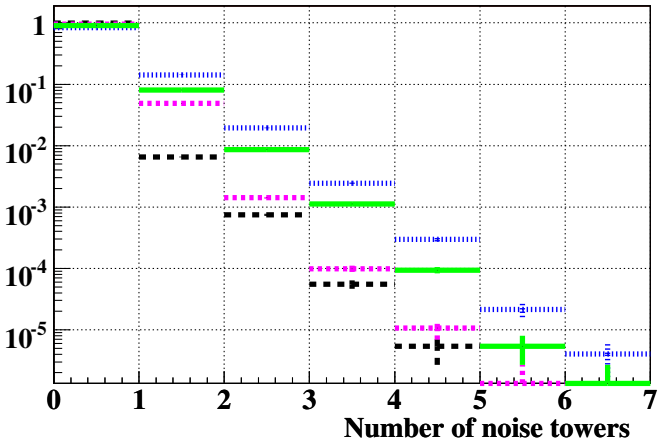

Figure 23: Number of noise towers satisfying (a) $P_T \geq 7$ GeV and $\eta < 1.8$ (pink) (b) 5 GeV $< P_T < 7$ GeV and $\eta < 1.8$ or $P_T \geq 5$ GeV and $1.8 \leq \eta < 2.6$ (green) (c) 4 GeV $< P_T < 5$ GeV and $\eta < 2.6$ or $P_T \geq 5$ GeV and $1.8 \leq \eta < 2.6$ (blue) (d) $P_T \geq 5$ GeV with $2.6 \leq \eta < 3.2$ (black).

1) *Total number of towers fired from jets in the event:*

Assuming that jets are separated enough so that their effect add linearly, the total number of fired towers per event coming from jets, called $N_{\text{event}}^{\text{jet}}$ is computed by adding to it the number of fired towers for each jet, called N_{jet}.

The number of tower above 7 GeV in each jet, $N7_{\text{jet}}$, is first computed by picking randomly a number in the distribution of tower above 7 GeV with $|\eta| < 1.8$ for the jet P_T using the corresponding two dimensional histogram. $N7_{\text{jet}}$ is then added to the total number of tower above 7 GeV in the event, $N7eta18_{\text{event}}^{\text{jet}}$. We proceed in the same way to obtain $N5eta26_{\text{event}}^{\text{jet}}$, $N4eta26_{\text{event}}^{\text{jet}}$ and $N5eta2632_{\text{event}}^{\text{jet}}$. Here it is worth to notice that the set of numbers is exclusive. For example, what we call $N5eta26_{\text{event}}^{\text{jet}}$

is the number of towers between 5 and 7 GeV with $|\eta| < 1.8$ or above 5 GeV with $1.8 < |\eta| < 2.6$, and not the number of tower above 5 GeV in $|\eta| < 2.6$.

2) *Total number of towers fired from noise in the event:*
We then add the effect of noise towers, N_{noise}, for each trigger region by picking a random number in each noise distribution previously measured:

$$\begin{aligned} \text{N7eta18}_{\text{event}} &= \text{N7eta18}^{\text{jet}}_{\text{event}} + \text{N7eta18}_{\text{noise}} \\ \text{N5eta26}_{\text{event}} &= \text{N5eta26}^{\text{jet}}_{\text{event}} + \text{N5eta26}_{\text{noise}} \\ \text{N4eta26}_{\text{event}} &= \text{N4eta26}^{\text{jet}}_{\text{event}} + \text{N4eta26}_{\text{noise}} \\ \text{N5eta2632}_{\text{event}} &= \text{N5eta2632}^{\text{jet}}_{\text{event}} + \text{N5eta2632}_{\text{noise}} \end{aligned}$$

3) *Total number of towers fired in the event:*
Finally, we compute the total number of towers satisfying each trigger term requirement:

$$\begin{aligned} \text{N7} &= \text{N718}_{\text{event}} \\ \text{N5} &= \text{N718}_{\text{event}} + \text{N526}_{\text{event}} + \text{N52632}_{\text{event}} \\ \text{N4} &= \text{N718}_{\text{event}} + \text{N526}_{\text{event}} + \text{N426}_{\text{event}} \end{aligned}$$

with N7 the total number of tower above 7 GeV in $|\eta| < 1.8$, N5 the total number of tower above 5 GeV in $|\eta| < 3.2$ and N4 the total number of tower above 4 GeV in $|\eta| < 2.6$.

For v10-13, the L1 term is fired if N5 ≥ 3.
For v14.0-7, the L1 term is fired if N5 ≥ 3 and N4 ≥ 3 .
For v14.8-, the L1 term is fired if N7 ≥ 1 and N5 ≥ 3 and N4 ≥ 3 .

4.1.4 Check of the method for L1

The method previously described was checked using an orthogonal subsample of the TOPJETTRIG skimming, requiring at least three good jets in each event. The probability to fire the different L1 conditions is predicted and compared with the true trigger firing, as one can see in figure 24.

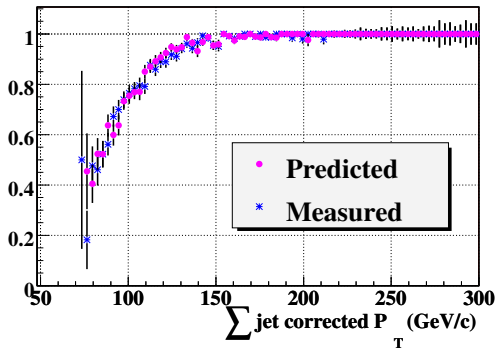

(a) V10-13: CJT(3,5,3.2) turn-on versus $H_T^{offline}$

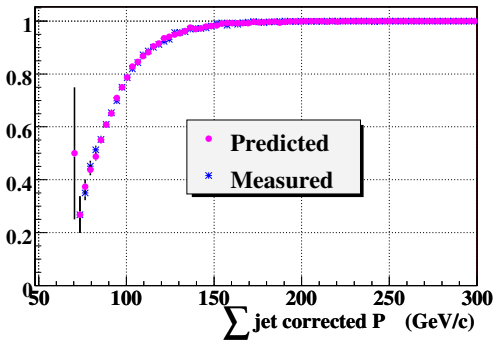

(b) V10-13: CJT(3,5,3.2) turn-on versus $H_T^{offline}$

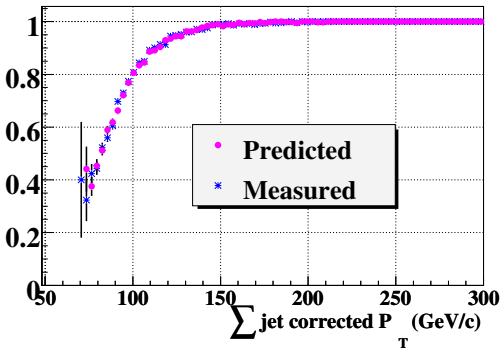

(c) V14.0-7: CJT(3,5,3.2)(3,4,2.6) turn-on versus $H_T^{offline}$

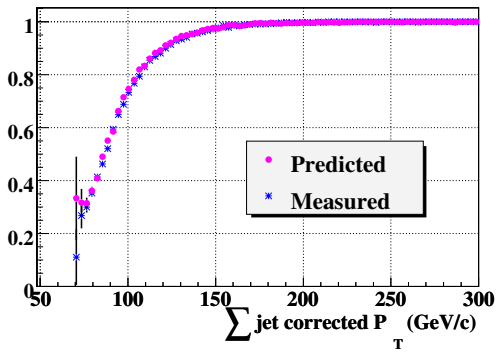

(d) V14.8-: CJT(3,5,3.2)(3,4,2.6)(1,7,1.8) turn-on versus $H_T^{offline}$

Figure 24: Comparison of the probability to fire L1 requirement measured in data (blue) and predicted using the method described in the text (pink).

4.2 Level 2

The L2 requirement of $h^0 b\bar{b}$ trigger consist of two sets of conditions: a condition on the L2 jet number and P_T, namely JT(x,y) with x the minimum number of L2 jets required and y their P_T threshold, and a condition on the scalar sum of the L2 jet P_T.

4.2.1 L2 jet requirement

Combining the effects of several jets at Level 2 is simpler than at Level 1, since at first order each reconstructed jet fires only one L2 jet. The number of L2 jet fired by a reconstructed jet can be seen in figure 25. As shown in 25, the probability to fire 2 L2 jets is around 1 %, so we will neglect it in the following.

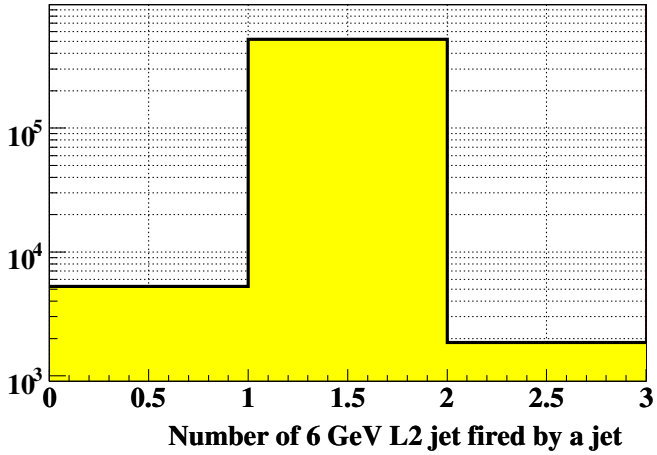

Figure 25: Number of L2 jets fired by a reconstructed jet in TOPJETTRIG sample, di-jet back to back event.

First, the effect of a single jet on L2 jets is studied. The sample previously described (two back to back jets and a triggered muon) is used. We look at the L2 jet near the jet. Looking at Figure 26 which shows the angular separation between the leading jet and the leading L2 jet, we see that a cut in ΔR of 0.5 should capture the L2 jets fired by the jet and minimize the chance to be sensitive to a possible unreconstructed jet.

The probability to fire a L2 jet above threshold (8 GeV for v10-11-12 and 6 GeV for v13-14) is measured as a function of the jet transverse momentum in three different calorimeter regions: $|\eta_{\rm jet}^{\rm det}| < 1.1$, $1.1 < |\eta_{\rm jet}^{\rm det}| < 1.5$ and $1.5 < |\eta_{\rm jet}^{\rm det}| < 2.5$, as shown in figure 27.

Now that the probability that a jet fired a L2 jet is known, it is straightforward to construct the probability to have x L2 jets above threshold in multi-jet events. After the first jet, the probability to fire exactly one L2 jet while the jet has a transverse momentum of P_{T1} is: $P(1, P_{T1}) = \text{Turn0n}(P_{T1})$ where Turn-On is the turn-on for the trigger list you want to simulate and for the calorimeter region of the jet. After the second jet of transverse momentum P_{T2}, the probability to fire exactly one L2 jet is $P(0,_{T1}) \times P(1, P_{T2}) + P(1,_{T1}) \times P(0, P_{T2})$ where $P(0,_{T1}) = 1 - \text{Turn0n}(P_{T1})$. We can proceed the same way for all the jets in the event:

$$P(= 1 \text{ L2 jet}) = \sum_{j=1}^{N_{jets}} P(1, P_{Tj}) \prod_{i=1, i\neq j}^{N_{jets}} P(0, P_{Ti}).$$

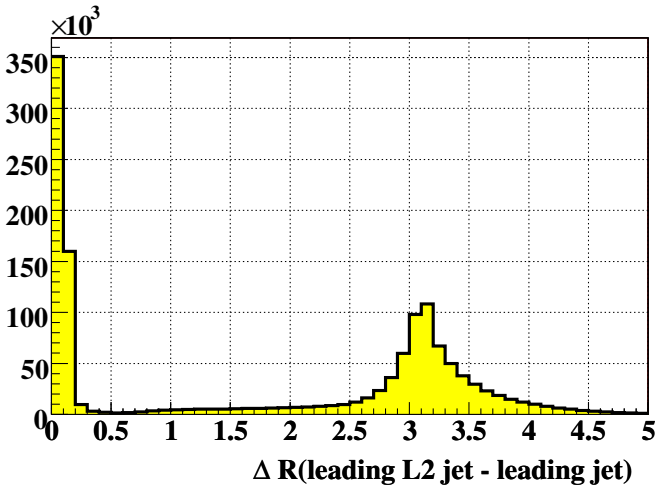

Figure 26: ΔR between the leading L2 jet and the leading jet. A cut at 0.5 is applied.

The probability to fire exactly two L2 jets is:

$$\mathrm{P}(=2\ \mathrm{L2\ jets}) = \sum_{\mathrm{j,k=1}}^{\mathrm{N_{jets}}} \mathrm{P}(1,\mathrm{P_{Tj}})\mathrm{P}(1,\mathrm{P_{Tk}}) \prod_{\mathrm{i=1,i\neq j,k}}^{\mathrm{N_{jets}}} \mathrm{P}(0,\mathrm{P_{Ti}}).$$

Finally, the probability to fire at least three L2 jets is given by:

$$\mathrm{P}(\geq 3\ \mathrm{L2\ jets}) = 1 - \mathrm{P}(=0\ \mathrm{L2\ jet}) - \mathrm{P}(=1\ \mathrm{L2\ jet}) - \mathrm{P}(=2\ \mathrm{L2\ jets})$$

4.2.2 Scalar transverse energy from L2 jets requirement

We still need to study the HT requirement at L2, i.e for v10-12 $\mathrm{HT_{L2}}(50,8)$ and for v13-14 $\mathrm{HT_{L2}}(70,6)$, where $\mathrm{HT_{L2}}(\mathrm{x,y})$ correspond to $\sum_{\mathrm{P_{TL2}>y}} \mathrm{P_{TL2}} > \mathrm{x}$. In multi-jet events from TOPJETTRIG skimming, we measure the probability to fire $\mathrm{HT_{L2}}(\mathrm{x,y})$ with respect to scalar transverse energy from jets. Figure 28 shows the probability to fire $\mathrm{HT_{L2}}(\mathrm{x,y})$ when the event already fired the L2 jet requirement.

The probability to fire $\mathrm{HT_{L2}}(\mathrm{x,y})$ is then directly obtained from the turn-on curve.

4.2.3 Check for L2

The final probability to fire the whole L2 requirement is given by:

$$\mathrm{P(N2)} = \mathrm{P(JT(3,z))} \times \mathrm{P(HT_{L2}(x,y))}$$

where z is the jet $\mathrm{P_T}$ threshold, x is the $\mathrm{HT_{L2}}$ threshold and y the $\mathrm{P_T}$ threshold of the jets used to build $\mathrm{HT_{L2}}$. As it was done in the previous section, this method is checked in an orthogonal TOPJETTRIG subsample requiring at least three jets. The prediction we obtained with our method is compared to the real trigger firing at L2 for each trigger list. These comparisons can be seen in Figure 29.

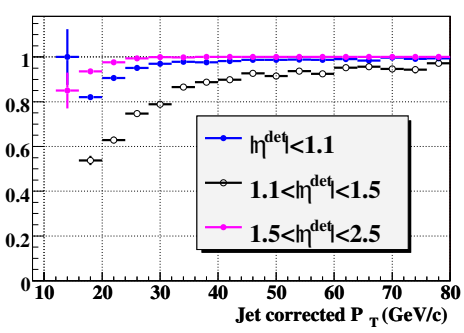

(a) V12

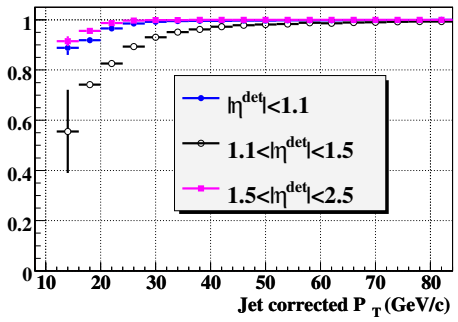

(b) V13

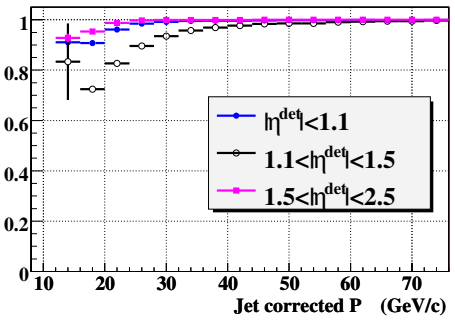

(c) V14

Figure 27: Probability to fire a L2 jet with respect to jet corrected P_T.

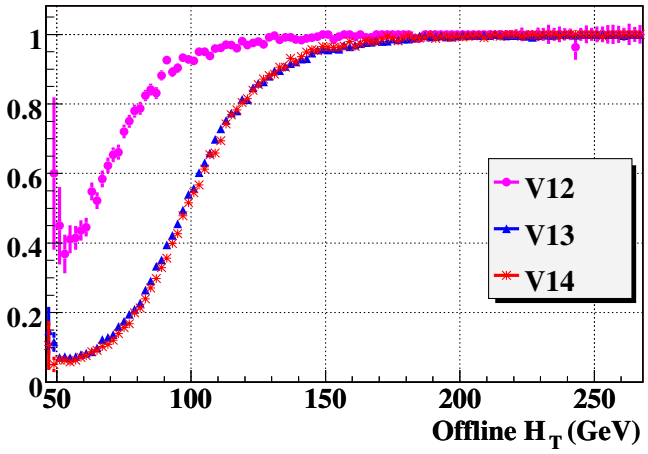

Figure 28: The probability to fire L2 HT(x,y) when JT(3,z) fired versus offline jes corrected H_T for each trigger list version.

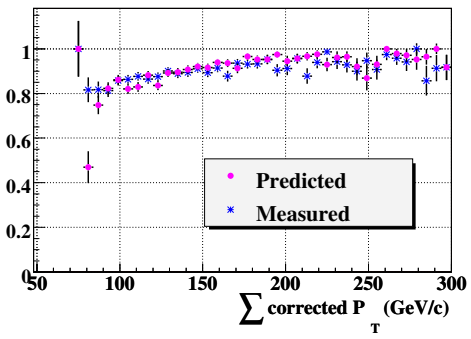

(a) V12: L2 JT(3,8) HT(50,8)

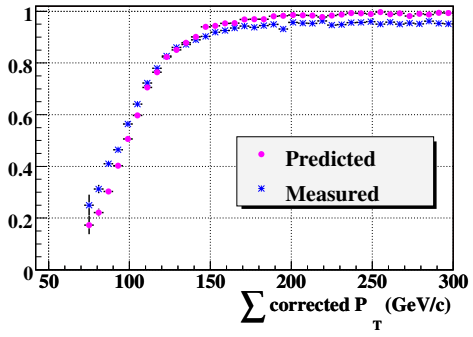

(b) V13: L2 JT(3,6) HT(70,6)

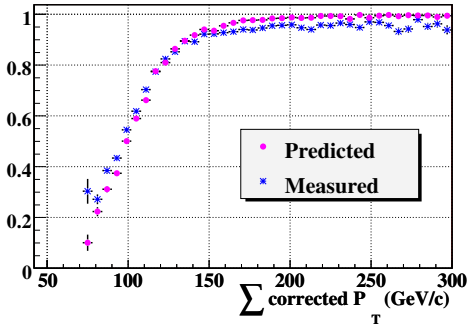

(c) V14: L2 JT(3,6) HT(70,6)

Figure 29: Comparison of the probability to fire the L2 requirement measured in data (blue) and prediction using our method (pink) versus scalar transverse momentum for jets.

4.3 Level 3

The L3 requirement of $h^0b\bar{b}$ trigger consists of two sets of condition:

1. a condition on the L3 jet number and P_T, namely JT(3,15) for v9 and v10 and JT(3,15)JT(2,25) for the other trigger lists;

2. a condition on the b content of the event. The significances of the impact parameter of the L3 tracks from the six leading L3 jets are combined using the same method as the way the JLIP probability is built. A probability, $L3^{evt}_{prob}$, that the event contains no b quarks is then computed and the requirement $L3^{evt}_{prob} < 0.05$ is applied at trigger level. A light jet probability, called $L3^{jet}_{prob}$ is also build for each L3 jet, using the significance of the tracks attached to them. This quantity is not used in $h^0b\bar{b}$ trigger, but will help us to compute L3 btag efficiency.

4.3.1 L3 jet requirement

The method used to compute the L3 requirement efficiency is the same than the one used for the L2 jet requirement. The sample used is still TOPJETTRIG back to back di-jet sample. All events are required to pass L1 and L2 $h^0b\bar{b}$ trigger requirement. L3 jets are matched to jets if $\Delta R_{jet,L3\,jet} < 0.5$. The ΔR distribution is shown in figure 30.

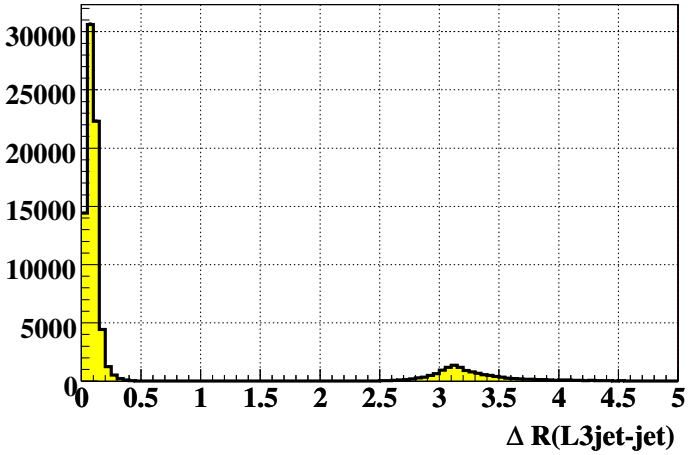

Figure 30: ΔR between L3 jets and jets. A cut at 0.5 is applied.

Since the probability to fire two 15 GeV L3 jets is around 0.01 % as one can see in Figure 31, it is neglected in the following.

The probabilities to fire a 15 GeV or 25 GeV L3 jet are measured with respect to the jet transverse momentum in three different calorimeter regions and for each trigger list, as one can see in Figure 32.

From the turn-on curves, the probability to fire JT(2,25) and JT(3,15) can be computed the same way it is done at L2. In the 3jets sub-sample, we predict the probability to fire L3 jet requirement of $h^0b\bar{b}$ trigger, that is $P(JT(2,25)) \times P(JT(3,15))$. This prediction is compared to the real L3 jet requirement $h^0b\bar{b}$ trigger firing. The agreement is good as can be seen in Figure 33.

Finally, a cut on the z position of the primary vertex is required in each event to ensure the PVZ term is fired: $|z_{PV}| < 35$ cm.

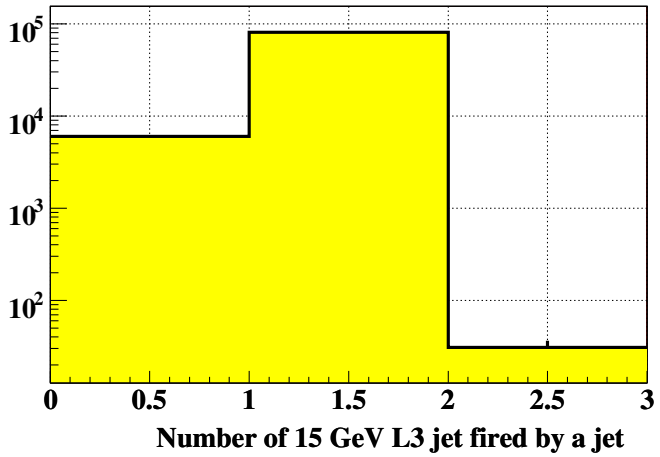

Figure 31: Number of 15 GeV L3 jets fired by a reconstructed jet in TOPJETTRIG di-jet back to back sample.

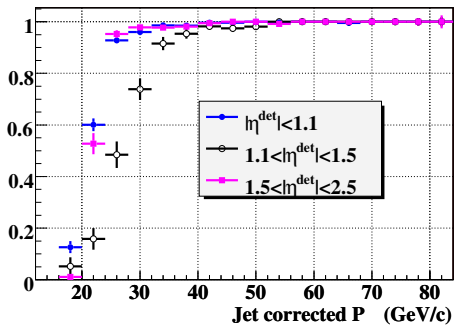

(a) V12

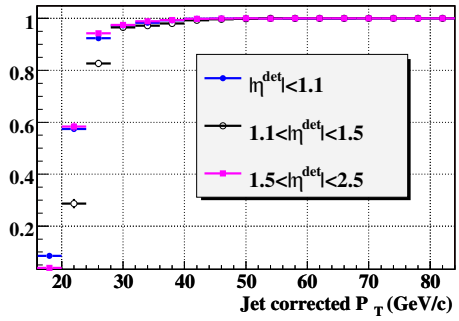

(b) V13

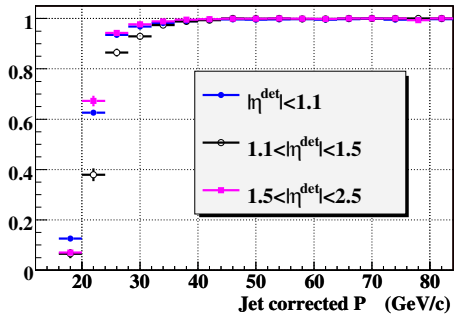

(c) V14

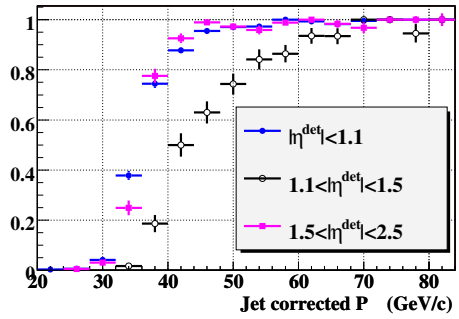

(d) V12

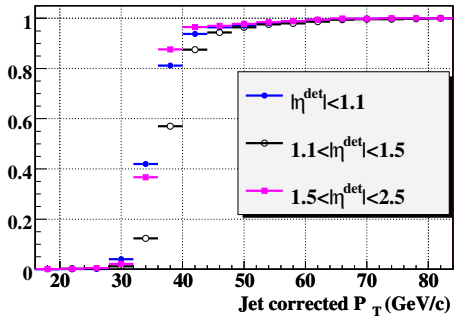

(e) V13

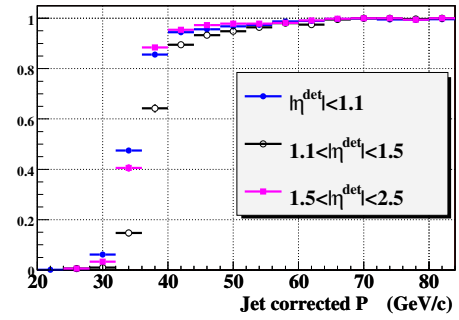

(f) V14

Figure 32: Probability to fire a 15 GeV (a)(b)(c) or a 25 GeV (d)(e)(f) L3 jet with respect to jet corrected P_T.

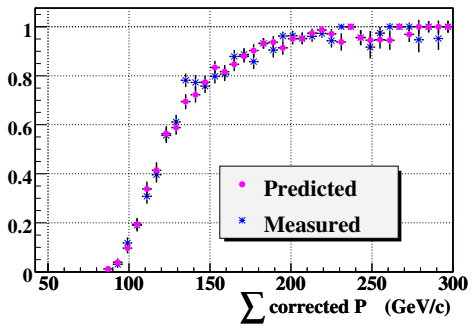

(a) V12

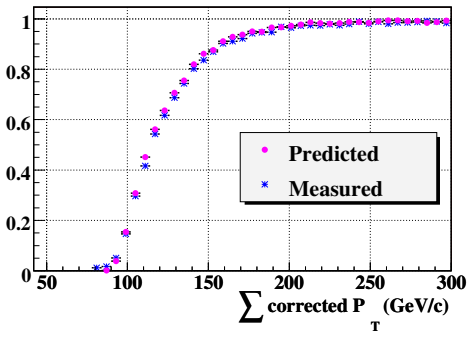

(b) V13

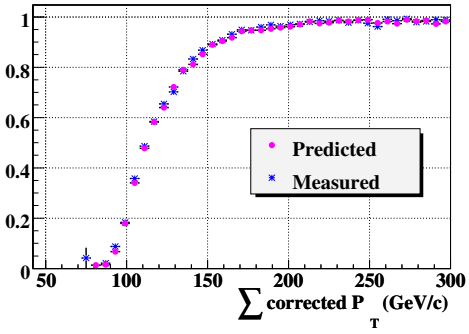

(c) V14

Figure 33: Comparison of the probability to fire the L3 jet requirement measured in data (blue) and predicted using our method (pink) versus scalar transverse momentum for jets.

4.3.2 L3 btag requirement

The first step is to simulate $L3^{jet}_{prob}$ distribution in Monte Carlo, using data and b-id methods. The sample is the p17 BID skim: at least one medium muon with $P_T > 4$ GeV and exactly 2 jets with $P_T > 10$ GeV. Each event is required to fire at least one trigger un-bbiased, and only runs from v13 or v14 are kept. We first look at SystemD [23], but due to a lack of statistics it was unusable. So we decided to use the "away jet" method, described in the following:

- **$L3^{jet}_{prob}$ for b jets**
  The method is based on the fact that a dijet event where one of the jet is b-tagged is likely to be a $b\bar{b}$ event. One of the jet is called the probe jet and the other the control jet.
  In this method, the probe jet contains a muon with P_T^{rel} above 0.7 GeV to enrich our sample in b jets. We then attempt to enhance furthermore the fraction of b jets by requiring the opposite jet (the away jet or the control jet) to be tight NN tag. The $L3^{jet}_{prob}$ distribution is obtained direclty from the probe jet. The resulting $L3^{jet}_{prob}$ distribution can be seen in Figure 34 (a).
  We also need to have $L3^{jet}_{prob}$ distribution for b-jet which satisfy a NN tight requirement. So we ask now the probe jet to be NN tight tag. The resulting $L3^{jet}_{prob}$ distribution can be seen in figure 34 (b).

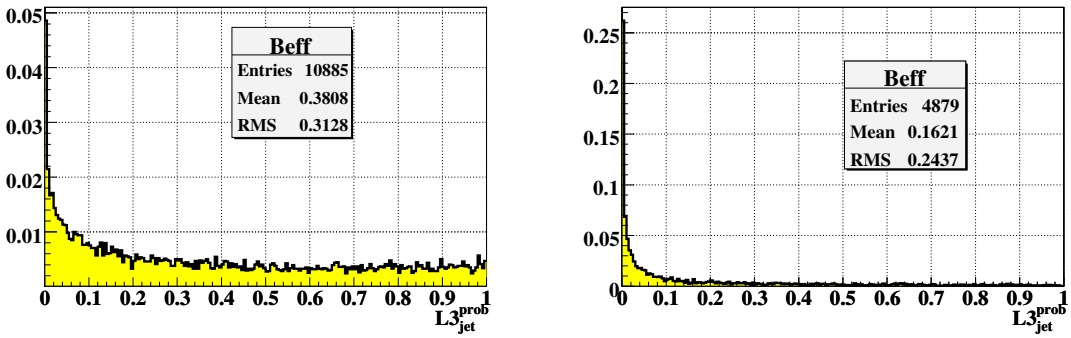

(a) (b)

Figure 34: $L3^{jet}_{prob}$ distribution for b jets obtained using away jet method, (a) asking the probe jet to be untagged, (b) asking the probe jet to be tagged.

- **$L3^{jet}_{prob}$ for light jets**
  The method used is based on the assumption that a dijet event where one of the jet is tightly negatively tagged is likely to come from light QCD production.
  The control jet is then tightly negatively tagged, and we look at the probe jet. The $L3^{jet}_{prob}$ distribution is obtained direclty from it, and can be seen in figure 35.

Now that we can simulate $L3^{jet}_{prob}$ for b and light jets in Monte Carlo, offline tagged or not, the next step is to define a new variable, $L3^{evt}_{probfromjet}$, that combine the L3 b-tag effect of all jets in the event:

$$L3^{evt}_{probfromjet} = \prod_i L3^{jet}_{prob} \times \sum_i \frac{(-\log \prod_i L3^{jet}_{prob})^i}{i!}.$$

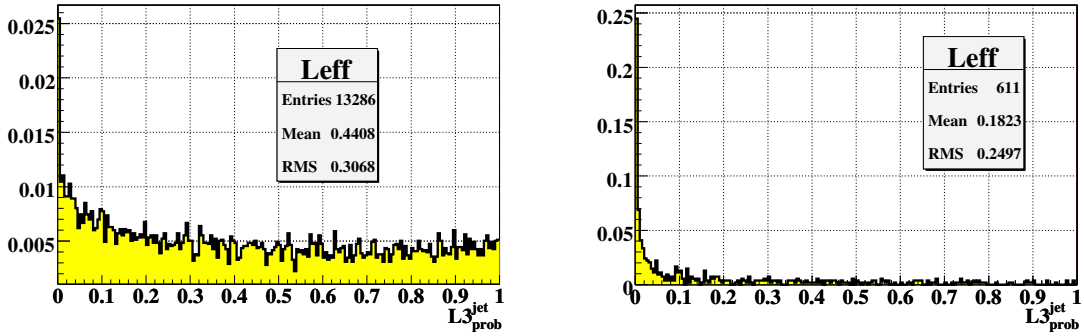

(a) (b)

Figure 35: $L3^{jet}_{prob}$ distribution for light jets obtained using away jet method, (a) asking the probe jet to be untagged, (b) asking the probe jet to be tagged.

Finally, the turn-on of L3 b-tag trigger is measured in TOPJETTRIG skim versus $L3^{evt}_{probfromjet}$, and is shown in figure 36.

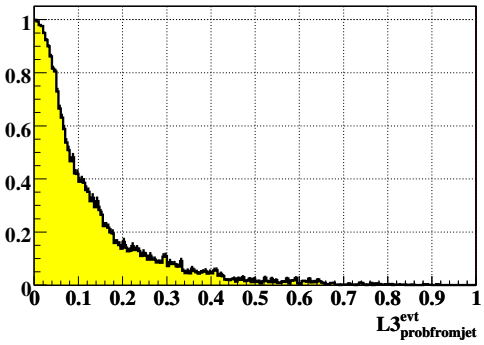

Figure 36: L3 btag turn-on versus $L3^{evt}_{probfromjet}$ in TOPJETTRIG event.

The probability to fire L3 btag is then directly obtained using the previous turn-on curve after having calculating $L3^{evt}_{probfromjet}$ using the different $L3^{jet}_{prob}$ distributions.

4.4 Efficiency in signal sample

The efficiency of $h^0 b\bar{b}$ trigger for each trigger list version are shown in table 8(a) for various signal samples and for the jet trigger term only. The efficiencies quoted are after the following set of analysis cuts:

- to simulate skimming cuts: we ask at least three jets with $P_T > 15$ GeV and one with $P_T > 20$ GeV in $|\eta| < 2.6$
- at least three and at maximum five good and taggable jets within $|\eta| < 2.5$ and satisfying $P_T > 15$ GeV;

- jes corrected transverse momentum of the leading jet above 40 GeV, of the second leading jet above 25 GeV and of the third leading jet above 15 GeV.

Now we require each event to have at least three NN tight b-tag jets.
The table 8(b) shows the efficiencies to pass l3btag requirement, when the jet requirements are fired. The table 8(c) summaries the overall trigger efficiencies including L3 b-tag for v13 and v14 trigger list.

Trigger List	**Higgs boson mass (GeV)**				
	100	**110**	**120**	**150**	**170**
v9	53.7 ±0.6	55.0±0.5	58.3±0.5	58.1±0.5	62.8±0.4
1 v10	60.8 ±0.5	61.6±0.5	64.4±0.5	62.9±0.5	66.5±0.4
v11/12	42.6±0.5	45.2±0.5	48.6±0.5	49.5±0.4	55.7±0.4
v13	45.5±0.5	47.7±0.5	51.7±0.5	52.6±0.4	58.2±0.4
v14.0-7	47.7±0.6	48.9±0.5	52.3±0.5	53.4±0.4	58.9±0.4
v14.8-9	47.3±0.5	49.2±0.5	53.7±0.5	54.3±0.4	60.0±0.4
Overall	46.1±0.6	46.9±0.5	51.3±0.5	53.0±0.4	58.3±0.5

(a)

Trigger List	**Higgs boson mass (GeV)**				
	100	**110**	**120**	**150**	**170**
v13	90±1	87±1	85±1	89±1	85±1
v14.0-7	87±1	87±1	85±1	86±1	86±1
v14.8-9	87±1	85±1	87±1	86±1	86±1

(b)

Trigger List	**Higgs boson mass (GeV)**				
	100	**110**	**120**	**150**	**170**
v9	87±2	86±1	86±1	85±1	85±1
v10	84±2	84±1	84±1	80±1	84±1
v12	58±2	62±2	65±2	70±1	74±1
v13	60±2	59±2	61±1	63±1	66±1
v14.0-7	58±2	62±2	63±2	63±1	67±1
v14.8-9	62±2	56±2	64±2	64±1	67±1
Overall	60±2	57±2	63±1	64±1	68±1

(c)

Table 8: Trigger efficiencies for various signal samples, (a) for jet terms only, (b) for l3btag terms only requiring at least three NN tight b-tag (c) for the averall terms. The quoted uncertainties arise from the limited MC statistics.

5 Triple b-tagged background calculation

The expected background used to set limit is calculated directly from data because of the high uncertainty on multi-jet processes cross-sections ($\approx 100\%$). In the double b-tagged sample, we compute the fraction of jets which are b-tagged excluding randomly two of them, outside the signal region ($\pm 1\sigma$ of the Gaussian fit to the signal mass distribution). This fraction will be called in the following "tag rate function", and can be seen in Figure 37 for a Higgs boson of mass 120 GeV.

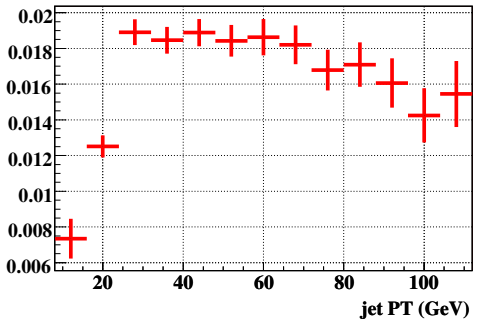

Figure 37: Fraction of jet which are b-tagged in double b-tagged sample, excluding randomly two of the b-tagged jets, for a Higgs boson mass of 120 GeV, using the NN tight working point.

It is worth to notice that the tag rate function, which is in fact the probability to b-tag a jet when there are already two b-tagged jets in the event, is stable between v9-12 and v13-14, as one can see in figure 38. However, this was not obvious because of the presence of a possible correlation between the jets due to the L3 b-tag per event in v13-14. In fact, the two NN tight b-tag are enough to assure that the L3 b-tag is fired, and the other jets are completely decorrelated with respect to b-tagging.

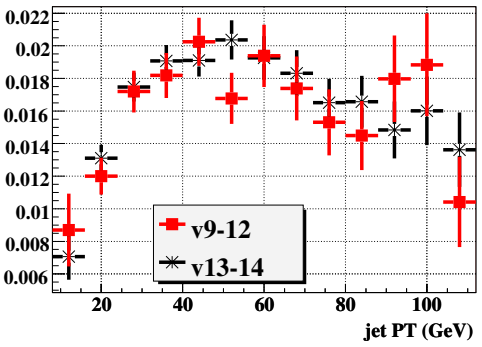

Figure 38: Fraction of jet which are b-tagged in double b-tagged sample, excluding randomly two of the b-tagged jets, for a Higgs boson mass of 120 GeV, using the NN tight working point, in v9-12 (red square) and v13-14 (black star).

For each event of the double b-tagged sample, the tag rate function is applied to the non b-tagged jets and the probability to have at least three b-tags jets is calculated. This triple b-tagged background calculation is normalized outside the signal region to the triple b-tagged sample, taking possible signal into account. In consequence this procedure is done during the limit setting procedure, for each tested $\tan\beta$.

This estimation of the background will be referred to as the "triple b-tag estimation".
The signal mean and width from the Gaussian fit can be seen in Table 9 and the Gaussian fit to the signal mass distribution for each Higgs boson masses is shown in Figure 39.

Higgs boson mass (GeV)	**100**	**110**	**120**	**150**	**170**
mean	104	107	111	130	143
width	26	25	22	28	32

Table 9: Means and widths of the Gaussian distributions fitted to the signal for each m_H.

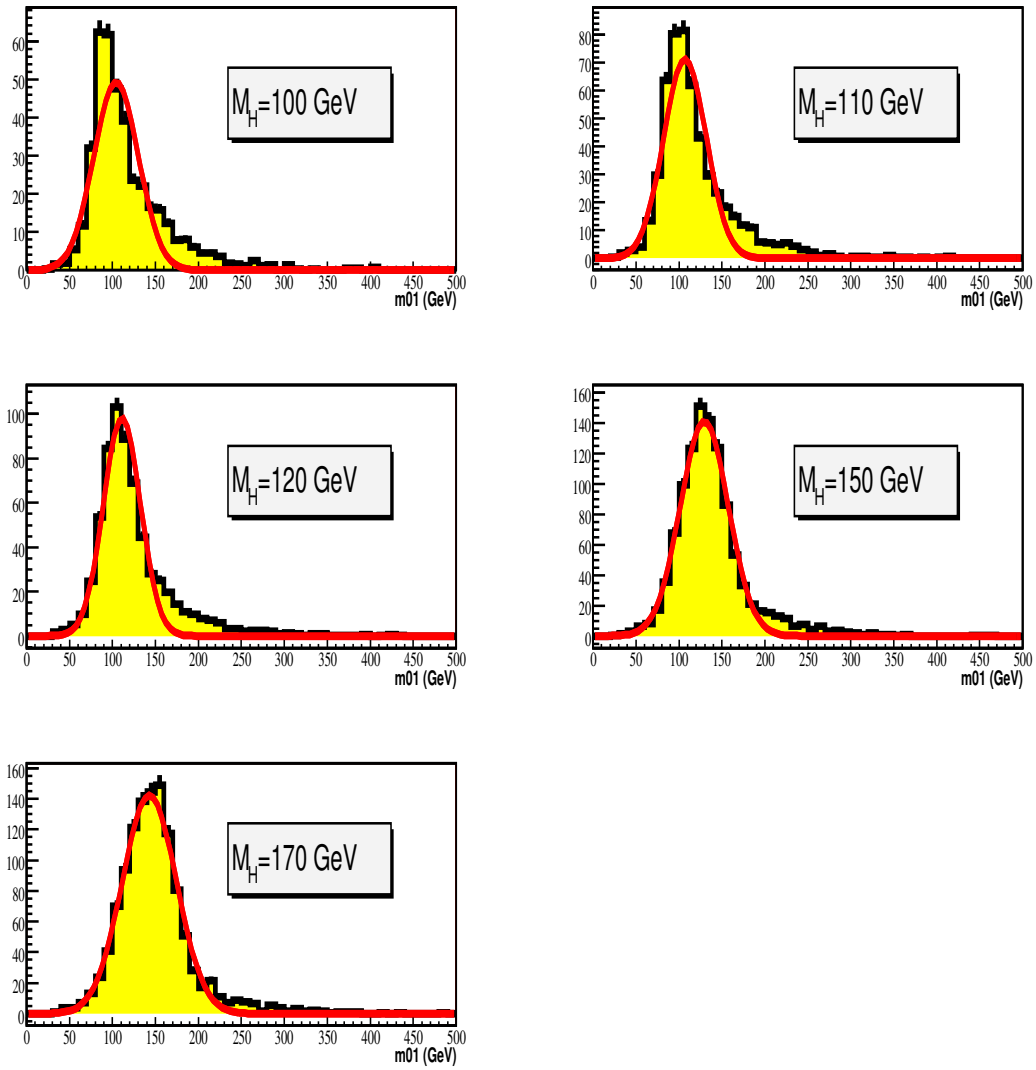

Figure 39: Invariant mass of the two leading jets distribution for each signal mass, after 3 b-tagged jets requirement, as well as the corresponding Gaussian fit.

6 Monte Carlo Cross-Checks

The comparaison of our data to Monte Carlo backgrounds provide an important cross-check of the trigger simulation method, of the jes correction and of the b-tagging. It is thus a necessary step for our analysis.

The multi-jet background is divided into 4 categories:

- jjj(j) production, calculated in data using the method described in section 6.1;
- bjj(j) production, calculated in data using the method described in section 6.1;
- bbj(j) production, simulated with ALPGEN as described in section 2.3;
- bbb(b) production, simulated with ALPGEN as described in section 2.3.

In the following we will refer to bbj(j) and bbb(b) backgrounds as "heavy multi-jet contribution".

6.1 Determination of $p\bar{p} \to jjj(j), bjj(j)$

As seen in section 2.3, the processes $p\bar{p} \to jjj(j), bjj(j)$ are difficult to simulate. However, because of their large cross-section, they contribute significantly to the background for the signal. In order to be able to compare Monte Carlo to data, they have to be determined. The method used is described in the following.

6.1.1 Neglecting bbj(j) events

In a first stage, we neglect the contribution of bbj(j) events.
The fraction of events from bjj(j) process is computed with the help of the matrix method, which consists in solving the following set of two equations with two unknowns:

$$N_{0tag}(n_{jets}) = N_{jjj(j)}(n_{jets}) + N_{bjj(j)}(n_{jets}) \quad (1)$$

$$N_{1tag}(n_{jets}) = n_{jets}.f.N_{jjj(j)}(n_{jets}) + (\epsilon + (n_{jets} - 1).f)N_{bjj(j)}(n_{jets}), \quad (2)$$

where N_{0tag} is the number of events with no b-tagging requirement and N_{1tag} the number of events with at least one NN loose b-tag jet, f is the mist-tag rate and ϵ the efficiency to tag a b-jet for the same working point. We neglect the fraction of events from the processes $p\bar{p} \to b\bar{b}j(j), b\bar{b}b(b)$, and we use the mist-tag rate and the b-jet efficiency given by the b-id group. In principle f and ϵ depend on the transverse momentum and the pseudo-rapidity of a given jet, but we are working on an event-by-event basis. The first input to these functions is taken as the average transverse momentum, $< P_T >$, in the event (Figure 40 (a)). The 2-dimensional (η, PT) distribution of the jets in our data samples (Figure 40 (b)) is used to randomly picked a value for η according to $< P_T >$.

The fraction of N_{bjj} obtained by this method, when the event has exactly 3, 4 or 5 jets is shown in Figure 41. It is worth to notice that the fraction of bbj(j) events in v13-14 is $\approx 35\%$ higher than in v9-12 due to the L3 b-tag requirement.

It was checked that the fraction of bjj event does not depend on the b-tagging working point used in the matrix method.

The second step consists in running on the data sample and deciding randomly if a given event is of type bjj(j) or a jjj(j) according to the expected fraction of bjj(j) event. If the event is a chosen as bjj(j) event, the probability the event has at least two or three b-tags is computed using the b-jet efficiency and the mist-tag rate from the b-id group. If the event is a chosen as jjj(j), the probability the event has at least two or three b-tags is computed using only the mist-tag rate from the b-id group.

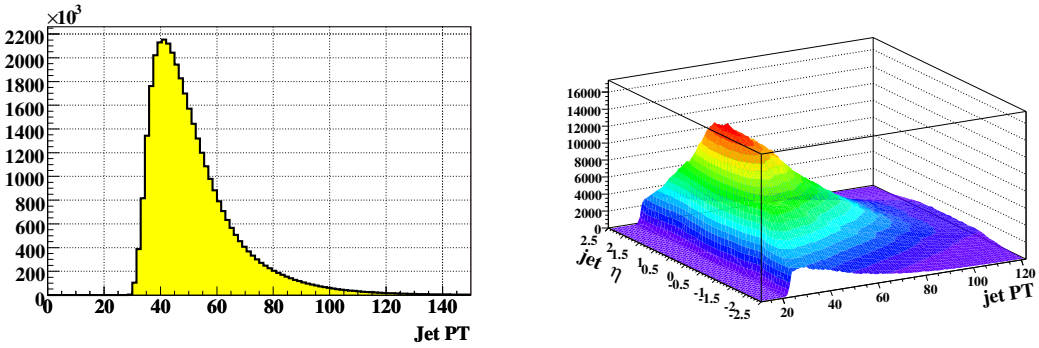

(a) (b)

Figure 40: (a) Mean P_T distribution. (b) $\eta - P_T$ map.

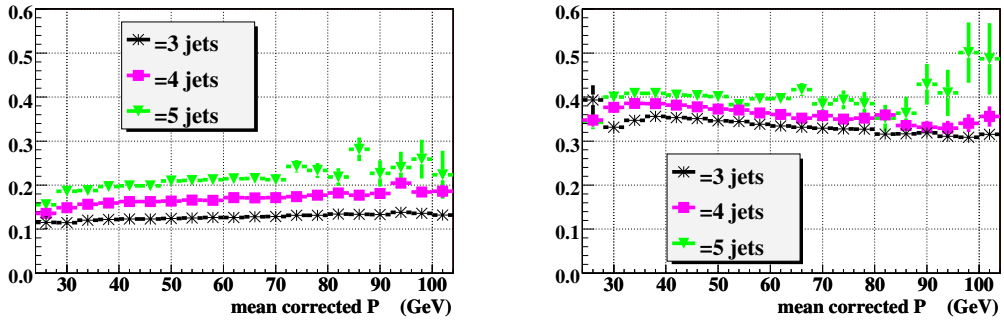

(a) V9-12 (without L3 b-tag requirement) (b) V3-14 (with L3 b-tag requirement)

Figure 41: Fraction of bjj(j) event versus mean P_T.

6.1.2 First comparison of data to expectations

We compare the invariant mass of the two leading jet in data and Monte Carlo, first requiring at least 2 b-tag jets and then requiring at least 3 b-tag jets. The "heavy multi-jet contribution" is normalized to the number of events in the double (triple) b-tagged data after subtracting the jjj(j) and bjj(j) estimated contributions. All the four backgrounds are then added and compared to the data if at least 2 b-tags are required, and to the "triple b-tag estimation" from section 5 when at least 3 b-tags are required.

The Monte Carlo cross-check of the double b-tagged data can be seen in figure 42 (a). The agreement is reasonable, and the "heavy multi-jet contribution" normalization factor from the double-tagged is 2.66 .The Monte Carlo cross-check of the triple b-tagged data is shown in figure 42 (b). The agreement is reasonable. The "heavy multi-jet contribution" normalization factor from the triple-tagged is 2.81.
The "heavy multi-jet contribution" normalization factor from the double and triple b-tagged data differ by 5 %. A possible cause of the discrepancy is that at this stage we neglect the amount of bbj(j) event, so we may slightly overestimate the tripple b-tagged bjj(j) contribution.

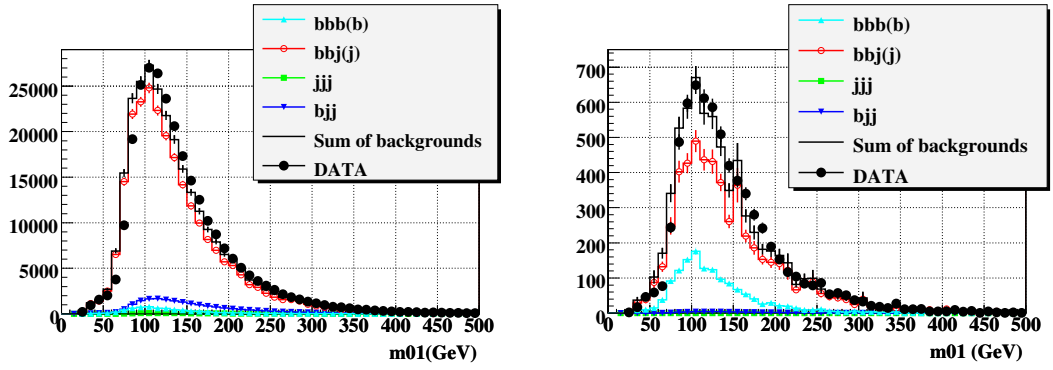

(a) (b)

Figure 42: Monte Carlo cross checks of the double b-tagged data (a) of the tripple b-tagged data (b).

6.1.3 Correcting for bbj(j) events

Now that we have en estimation of the bbj(j) contributions, the fraction of events in data that was due to these events is estimated and included in the matrix method.
The fraction of bbj(j) events in 0-tagged data is obtained from the Monte Carlo bbj(j) rescaled with the normalization factor from the double tagged data. The fraction of bbj(j) events is egal to 3.7 % in v9-12 and to 6 % in v13-14.

Then the equations 1 2 become:

$$\begin{aligned} N_{0tag}(n_{jets}) &= N_{jjj(j)}(n_{jets}) + N_{bjj(j)}(n_{jets}) + N_{bjj(j)} \\ N_{1tag}(n_{jets}) &= n_{jets}.f.N_{jjj(j)}(n_{jets}) + (\epsilon + (n_{jets} - 1).f)N_{bjj(j)}(n_{jets}) + \epsilon_{1tag}.N_{bjj(j)}, \end{aligned}$$

where ϵ_{1tag} is the probability to tag at least 1 jets in Monte Carlo bbj(j) sample. It is egal to 0.7. We then do the same than in section 6.1.1. The final fraction of bjj(j) events is shown in figure 43.

The contribution of jjj(j) and bjj(j) is then computed the same way it is done in section 6.1.1.

6.1.4 Final comparison of data to expectations

We can now compare our data to expectations using the corrected jjj(j) and bjj(j) predictions. As before, the "heavy multi-jet contribution" is normalized to the number of events in data after substracting the contribution of jjj(j) and bjj(j) productions. The Monte Carlo cross-check of the double b-tagged data can be seen in figures 44 . The agreement is reasonable.
The "heavy multi-jet contribution" normalization factor from the double-tagged is 2.72.

We also compare the invariant mass spectrum of the two leading *b-tagged* jets in the double b-tagged data to background estimation, as shown in figure 45. The peak at low invariant mass, present in data dominated by the bbj(j) production, is likely due to gluon-splitting events. The normalization of the "heavy multi-jet contribution" is egal also egal to 2.72, as the one derived in the two leading jets invariant mass spectrum. This give us confidence in the modelisation of the backgrounds.

The Monte Carlo cross-check of the triple b-tagged data is shown in figures 46. The agreement is reasonable. The "heavy multi-jet contribution" normalization factor from the triple-tagged is 2.82.

The "heavy multi-jet contribution" normalization factor from the double and triple b-tagged data differ now by 3.9 %. The slight difference between these two factors can be due to the possible presence

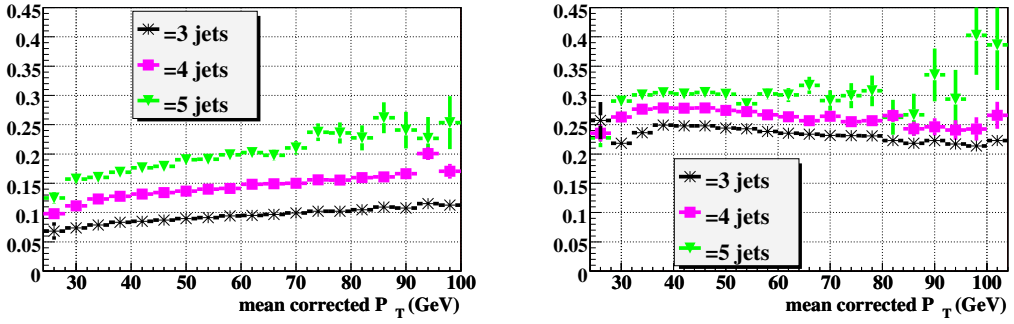

(a) V9-12 (without L3 b-tag requirement)

(b) V3-14 (with L3 b-tag requirement)

Figure 43: Fraction of bjj(j) event versus mean P_T after correcting for bbj(j) events.

of c quakrs, that we neglect. Another possible cause is the correlation with respect to offline b-tagging between the jets, that is introduce in v13-14 by the L3 b-tagger. It was not taken into account when calculating the total number of bjj(j) and jjj(j) events in double or triple b-tagged data.

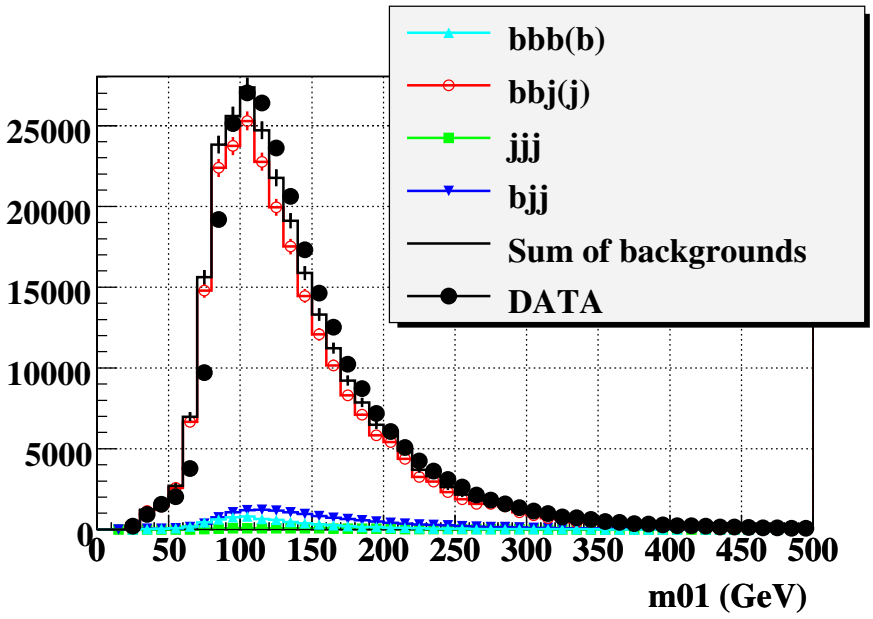

(a) linear scale

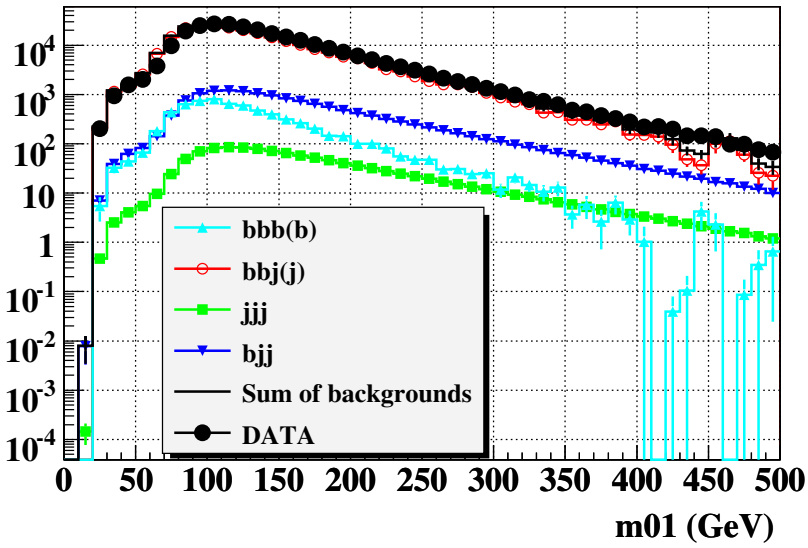

(b) logarithmic scale

Figure 44: Monte Carlo cross checks of the double b-tagged data's two leading jet invariant mass spectrum, after correctiong for bbj(j) contribution while calculating jjj(j) and bjj(j) productions.

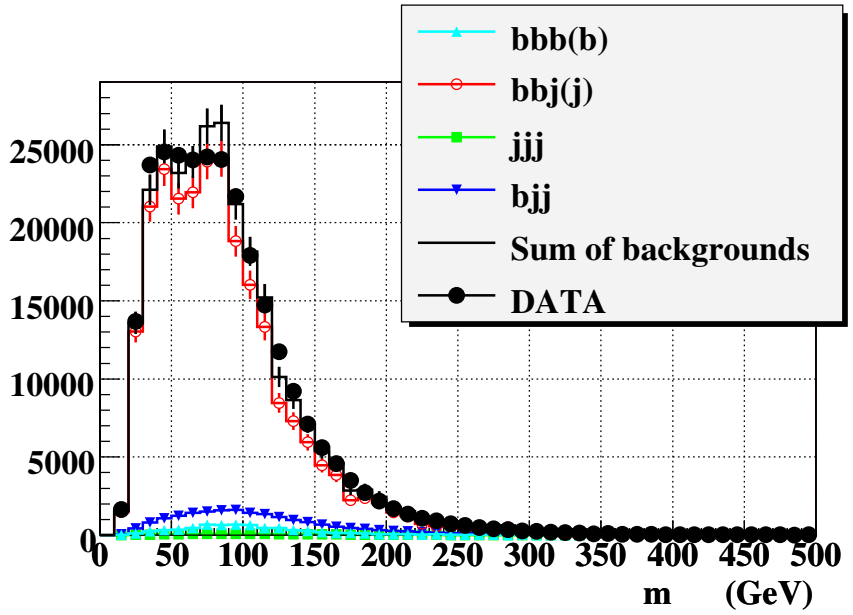

Figure 45: Monte Carlo cross checks of the double b-tagged data's *two leading b-tagged jet* invariant mass spectrum, after correctiong for bbj(j) contribution while calculating jjj(j) and bjj(j) productions.

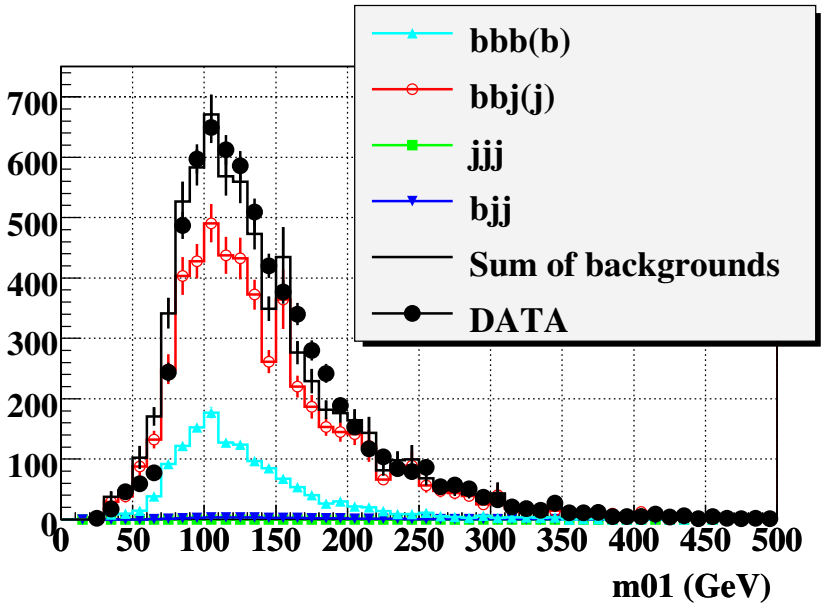

(a) linear scale

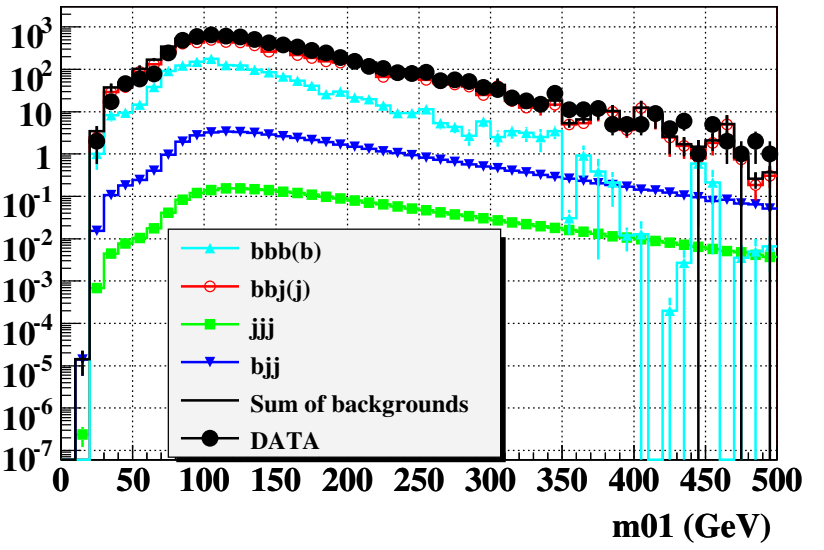

(b) logarithmic scale

Figure 46: Monte Carlo cross checks of the triple b-tagged data's two leading jet invariant mass spectrum, after correctiong for bbj(j) contribution while calculating jjj(j) and bjj(j) productions.

7 Systematic Errors

Several sources of systematic errors have been identified, and they can be separated in two categories:

- errors affecting the calculation of signal acceptance and yield,
- errors affecting the number of estimated background events.

7.1 Signal Systematics

The errors from all sources which affect the signal acceptance and yield are added in quadrature and are summarized in Table 10.

The uncertainty on the determination of the integrated luminosity for the data sample is 6.5 %.

An uncertainty arises from an imperfect understanding of the signal generation due to the limited order in perturbation theory at which signal events are generated (semi-LO for Pythia) and at which total cross sections are calculated (NLO). Simulated event were weighted to match NLO P_T and η spectra, as described in section 1. Since the procedure is only an approximation to reproducing the full NLO kinematics of the events, an error is assigned of 5 % in average.

The remaining source of theoretical error is the extend to which the NLO cross-sections of perturbation theory differs from the one summing all orders. The magnitude of the error is estimated by varying various parameter as the renormalization and factorization scales of the NLO cross-section calculation, as described in section 1.

The jet trigger efficiency is subject to errors coming from the different topologies between a multi-jet event and a di-jet event, events which are used to measure trigger turn-ons, from the assumption that jet can fire only one L2 or L3 jet, that the triggered jets are independent. The error can be estimated from the difference between our predictions and the true trigger firing (figures 24, 29, 33). The ratio, "R", of the predicted and the measured histograms is computed with respect to offline transverse energy from jets at all trigger levels. Then each signal event is weighted by $R_{L1} * R_{L2} * R_{L3}(H_T)$. This systematic is on average 3 %.

There is also a systematic from the L3 b-tag efficiency. We assume that the L3 b-tag turn-on versus $L3^{evt}_{probfromjet}$, measured in TOPJETTRIG skim, is independent with respect to the number of offline b-tag jets in the event. This is not true, as shown in figure 47.

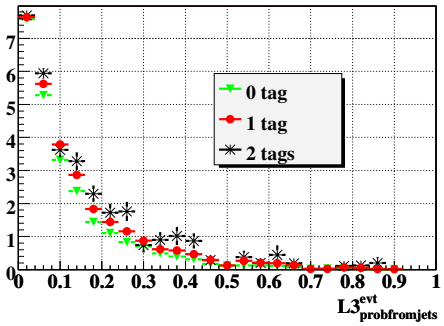

Figure 47: L3 btag turn-on versus $L3^{evt}_{probfromjet}$ in TOPJETTRIG event for 0 tag, at least 1 b-tag and at least b-3 tags.

Using the turn-on obtained in the double b-tagged TOPJETTRIG sample give a systematic error of 2 %.

Higgs boson mass (GeV)	**100**	**110**	**120**	**150**	**170**
Lumi	6.5	6.5	6.5	6.5	6.5
Theoretical	12.3	12.0	12.1	13.0	13.5
Trigger	4.0	4.9	3.6	4.2	2.5
ID	0.3	0.5	0.4	0.4	0.4
JES	4.8	4.6	3.9	2.8	2.7
Reso	0.6	0.2	0.1	0.3	0.5
JET	4.9	4.7	3.9	2.8	2.8
b-ID	8.1	8.2	8.3	8.8	9.3
Total	17.2	17.3	17.0	17.7	18.0

Table 10: The errors from each source (in %) which are added in quadrature to give the total errors on acceptance.

A second source of systematic error in the calculation of the L3 b-tag efficiency is the method we used to derive $L3^{jet}_{prob}$. The "away jet" method used to obtain $L3^{jet}_{prob}$ for b jets is contaminated by light jet. So the cut of 0.7 GeV on the muon P^{rel}_T is increased to 1.5 GeV, and a megatight requirement is applied on the control jet, instead the tight working point previously used. The "away jet" method used to obtain $L3^{jet}_{prob}$ for light jets is contaminated by b jet. So we measured the $L3^{jet}_{prob}$ in 3JET skimming, requiring the jets to be negatively tagged or to be not tagged. The analysis is then rerun using the new $L3^{jet}_{prob}$ distributions and it gives an uncertainty of 1 %.
We add in quadrature the uncertainty from jet term and b-tag term. The overall trigger systematic is then around 4 %.

The uncertainty on the b-tagging efficiency in data is taking into account in the error on the b-jet efficiency and the mist-tag rate provided by the BID group. This error is parametrized as a function of jet P_T and η. So the analysis was run using $\pm 1\sigma$ in the value of the b-jet efficiency and the mist-tag rate. The resulting acceptance uncertainty is around 8.5 %.

Possible discrepancy in jet identification efficiency, jet energy resolution, and jet energy scale, between DØ full simulation and the real data are addressed by the SSR method[20]. This method consists in comparing the jet reconstruction for $\gamma + j$ events and $Z + j$ events in both data and MC, to determine resolution, energy scales and jet-id efficiency. Systematic uncertainties in the results arise for example from limited statistics, differences observed between the $\gamma + j$ and $Z + j$ samples, or when varying the photon selection purity. To propagate these uncertainties, the signal acceptance has been computed after varying respectively the jet-id efficiency, the energy scaling and the jet resolution, within the provided assymetrical uncertainties. Each of the three errors are symmetrized by averaging the upper and lower observed variations. The three uncertainties obtained this way are then summed quadraticaly. There are quoted in Table 10 under the name "JET".

7.2 Background systematics

Background systematics are summarized in table 11.
There is a statistical error associated with the uncertainty in the normalization of the background: the error is given by $1/\sqrt{N_{event}}$ where N_{event} is the number of events in the "triple b-tag estimation" outside signal window.
There is also an additional systematic from the tag rate function, since this function is used to propagate the shape of the double b-tagged data to the triple b-tagged data. To estimate it, the shape of the double b-tagged data is used for the "triple b-tag estimation", instead of applying the tag rate function in the double b-tagged data to the non b-tagged jet. The difference between the number of events from this

Higgs boson mass (GeV)	**100**	**110**	**120**	**150**	**170**
Alternate method	1.8	2.3	2.4	1.9	1.9
Due to normalization	1.8	1.7	1.7	1.7	1.7
Total	2.4	2.8	2.8	2.6	2.6

Table 11: The errors from each source (in %) which are added in quadrature to give the total background systematics.

Higgs boson mass (GeV)	**100**	**110**	**120**	**150**	**170**
Kinematic	31	35	39	40	43
BID		8.8	9.7	9.9	9.2
Trigger	61	64	64	64	67

Table 12: The relative acceptance (in %) of selection cuts for signal for each Higgs masses.

two "triple b-tag estimation" give the systematic uncertainty.

8 Results

Table 12 shows the signal acceptance for each selection cuts and masses.

The trigger and kinematic efficiencies rise slightly with higgs mass, while the b-tagging efficiencies are stable, as expected.

Table 13 summarizes the final number of events in the double and triple NN tight b-tagged data, as well as the expected number of background events for each signal mass.

As no excess is seen in the data, limits on $\tan\beta$ are calculated using the full leading di-jet invariant mass shapes of the signal, expected background and data sample. The background is the triple b-tag estimation described in subsection 5. The CL_S method, implemented in TLimit, is employed to interpret the data. The effects of systematic uncertainties σ are taken into account by smearing the number of signal (or background) events with a Gaussian of width σ in toy MC experiment.
The signal histogram, derived assuming $\tan\beta = 1$ is scaled by $\tan\beta^2$. The value of $\tan\beta$ is increased, starting at 25, until the CL_S obtained is less than 5 %.

Figure 48 shows the data, the normalized background and the Higgs signal for two higgs masses (120 GeV and 170 GeV) at the observed 95 % CL exclusion limit.

Selection before b-tagging	19×10^6				
2 b-tags	269870				
3 b-tags	6749				
Higgs boson mass (GeV)	**100**	**110**	**120**	**150**	**170**
Normalization factor	0.997	0.993	0.992	0.992	0.990
Expected background	6947	6928	6926	6845	6687

Table 13: The final number of events in the double and triple b-tagged data, and the expected background to the triple b-tagged data, as well as the normalization of the expected background. NN tight b-tagged is used.

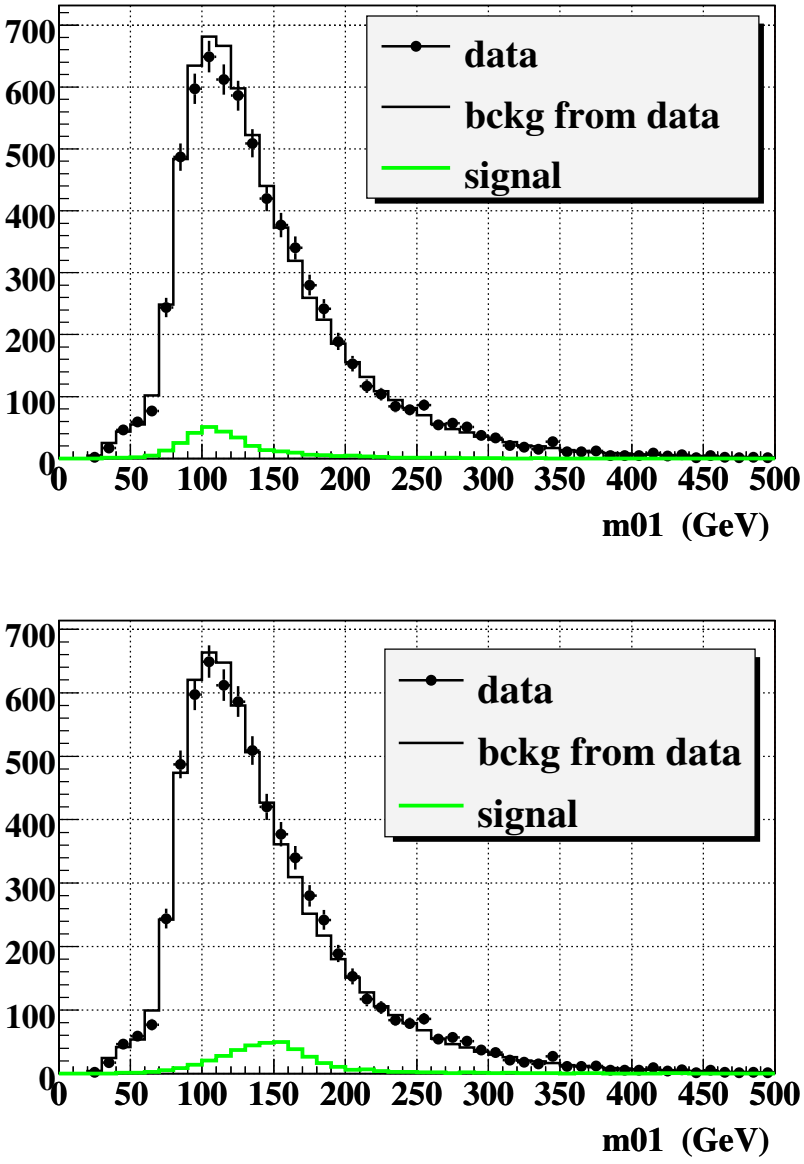

Figure 48: The data (circles), the normalized background (solid line) and the Higgs signal for $m_A = 120$ GeV at the observed 95 % CL exclusion limit ($\tan\beta = 60$) (top) and for $m_A = 170$ GeV at the observed 95 % CL exclusion limit ($\tan\beta = 121$).

Table 14 and Figure 49 show the observed and expected 95 % CL exclusion limits in the plan $\tan\beta - m_A$ that we are able to exclude with the current data. The sensitivity decreases with m_A, as expected since the signal cross-ection decreases with the Higgs boson mass.

Figre 50 shows the observed and expected 95 % CL limits on standard model $bh^0 \rightarrow b\bar{b}$ cross section as a function of m_A.

Higgs boson mass (GeV)	**100**	**110**	**120**	**150**	**170**
Observed $\tan\beta$ limit	46	57	60	85	121
Expected $\tan\beta$ limit	50	58	62	84	104

Table 14: The observed and expected 95 % CL exclusion limits in the $\tan\beta - m_A$ plane at tree level in the MSSM.

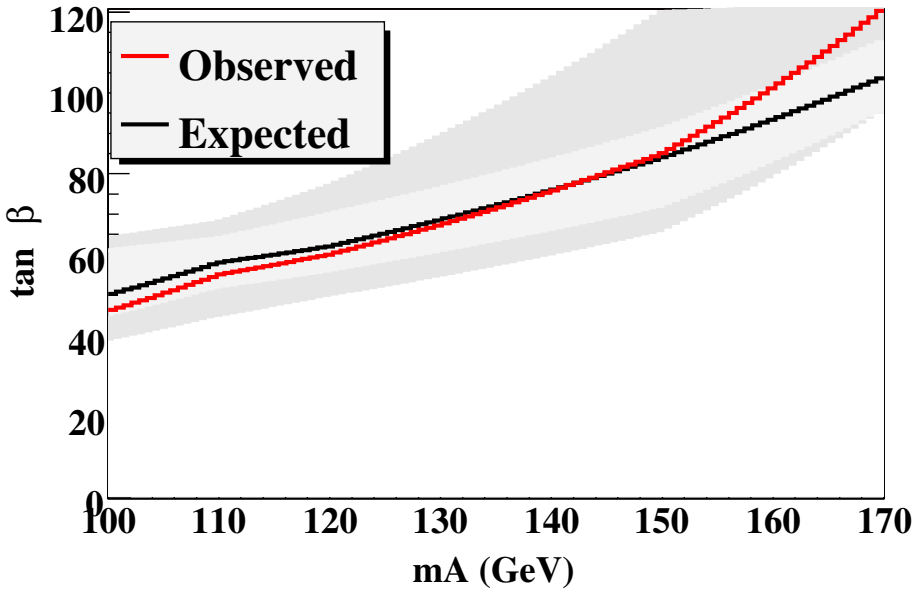

Figure 49: The observed and expected 95 % CL limits on $\tan\beta$ as a function of m_A, assuming $\tan\beta^2$ cross section enhancement. The error bands indicate the $\pm1\sigma$ and $\pm2\sigma$ range of the expected limit.

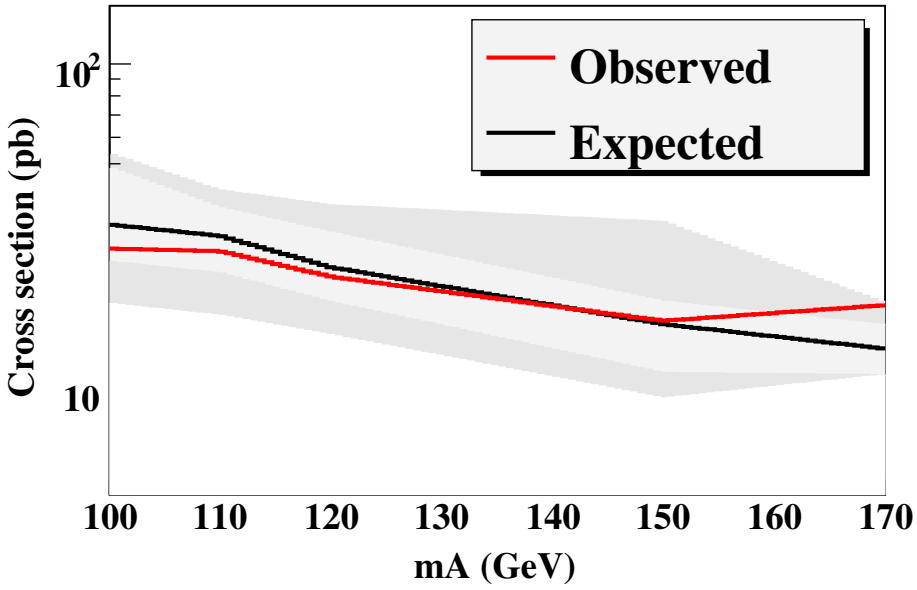

Figure 50: The observed and expected 95 % CL limits on standard model $bh^0 \rightarrow b\bar{b}$ cross section as a function of m_A. The error bands indicate the $\pm 1\sigma$ and $\pm 2\sigma$ range of the expected limit.

References

[1] S. Dawson *et al.*, *Higgs boson production with one bottom quark jet at hadron colliders*, hep-ex/0408077

[2] LEP Higgs Working Group (July 2005), Note2005-01
http://lephiggs.web.cern.ch/LEPHIGGS/papers/index.html

[3] The CDF collaboration, Phys. Rev. Lett. **86** (2001) 4472.

[4] The DØčcollaboration, Phys. Rev. Lett. **95** (2005) 15801.

[5] Andrew Hass, Avto Kharchivala, Marine Michaut, Jyothsna Rani, Tim Scanlon, Boris Tuchming *DØ Search for Neutral Higgs Bosons at High tan β in Multi-jet Events Using p14 Data*, DØ note 4671

[6] The CDF collaboration, Phys. Rev. Lett. **96** (2006) 011802.

[7] The DØčcollaboration, hep-ex/0605009.

[8] T. Sjostrand, L. Lonnblad, S. Mrenna and P. Skands, *Physics and manual*, hep-ph/0308153. We use Pythia 6.323.

[9] J.M. Campbell, R.K. Ellis, F. Maltoni and S. Willenbrock, *Higgs boson production in association with a single bottom quark*, hep-ph/0204093

[10] J.M. Campbell *et al.*, *Higgs boson production in association with bottom quarks*, hep-ph/0405302

[11] J.M. Campbell, R.K. Ellis, http://mcfm/.

[12] S. Dittmaier, K. Kramer and M. Spira, hep-ph/0309204

[13] S. Dawson, C. Jackson, L. Reina and D. Wackeroth, Phys. Rev. D **69** (2004) 074027.

[14] J.Pumplin *et al.*, *New generation of Parton Distributions with Uncertainties from Global QCD analysis*, hep-ph/0201195.

[15] http://www-clued0.fnal.gov/∼kehoe/l1cal/CalRunRanges.txt

[16] http://www-d0online.fnal.gov/www/groups/lum/reports/runs

[17] http://www-d0.fnal.gov/Run2Physics/higgs/d0_private/triggers/higgstrig.html

[18] Common Analysis Format web: page http://www-d0.fnal.gov/Run2Physics/cs/caf/

[19] M. L. Mangano, M. Moretti, F. Piccinini, R. Pittau and A. D. Polosa, "ALPGEN, a generator for hard multiparton processes in hadronic collisions," JHEP **0307**, 001 (2003) [arXiv:hep-ph/0206293].

[20] Nikola Makovec and Jean-Francois Grivaz, *Shifting, Smearing and Removing Simulated Jets*, DØ Note 4914

[21] S. Hoche, F. Krauss, N. Lavesson, L. Lonnblad, M. Mangano, A. Schalicke and S. Schumann, "Matching parton showers and matrix elements," arXiv:hep-ph/0602031.

[22] A. Hass, *DØ Level 1 and Level 2 calorimeter Trigger Performance in Multi-jets Events*, DØ Note 4073

[23] B. Clément et al., *SystemD or how to get signal, background and their effiencies with real data only*, DØ Note 4159

[24] A. Harel, *Jet ID optimisation*, DØ Note 4919

[25] T. Scanlon, *A Neural Network b-tagging Tool*, DØ Note 4889

[26] T. Scanlon and M. Anastasoaie, *Performance of the NN b-tagging Tool on Pass 2 p14 Data*, DØ Note 4890